Development of carbon yolk-shell magnetic nanoparticles by a novel eco-friendly approach for the removal of organic micropollutants by catalytic wet peroxide oxidation

Arnaldo Vinicius Dias Paes

Thesis report presented to

Escola Superior de Tecnologia e Gestão

Instituto Politécnico de Bragança

to obtain a master's Degree in

Chemical Engineering

within the scope of the double diploma with

Universidade Tecnológica Federal do Paraná

Supervisors:

Prof. Helder Teixeira Gomes

Profª. Ana Maria Ferrari

Dr. Jose Luis Diaz de Tuesta Triviño

Bragança

2022

ACKNOWLEDGEMENTS

Firstly, I would like to thank my family for all the unconditional support provided throughout these years. Supporting me in my decision to study abroad in search of new opportunities and challenges. Without you I would not have got where I am now.

Thanks to my supervisors Helder Teixeira Gomes, Jose Luis Diaz de Tuesta Triviño and Ana Maria Ferrari for all the support, help and guidance provided throughout the execution of this work.

A special thanks to my friends Adriano Santos Silva, Fernanda Fontana Roman, Larissa de Grande Piccinin and Gabriel de Freitas. You provided me one of the best working environments I have ever had the opportunity to work in, your help was essential for the completion of this work. To my friend of all times, Ana Paula Ferreira da Silva, you were extremely important in my personal and academic life, guiding me and providing all possible advice throughout this journey.

To my eternal friends with whom I had the pleasure of living daily, Gustavo Funchal, Victoria Melo, Lucas Cavichi, Cristiane de Carli, Gabriel Ribeiro, Lucas Fenato, Mariana Moia, Diogo Salvati and Daniela Elsenbach.

To my best friends Gabriel Ribeiro, Mariana Magalhães Moia and Nayra Caldas dos Santos. Thank you for always being present in my life, regardless of time and circumstances. Thank you for the advice, laughs,and venting. Thank you for sharing life with me and for providing me one of the best experiences I have ever had in my entire life.To all my friends from Brazil and Portugal, who were present directly and indirectly, giving me strength and support throughout this year.

Finally, I thank to UTFPR Apucarana and IPB for the space provided to carry out the activities and for providing me the opportunity to obtain a double degree.

This work was financially supported by UIDB/00690/2020 (CIMO), LA/P/0045/2020 (ALiCE), UIDB/50020/2020 (LSRE-LCM), and the project RTChip4Theranostics, with the reference NORTE-01-0145-FEDER-029394

ABSTRACT

This work addresses the carbon coating of magnetic nanoparticles based on cobalt ferrites ($CoFe_2O_4$) through a traditional method ($CoFe_2O_4$@RF), a greener method ($CoFe_2O_4$@PG) and their subsequent functionalization in CWPO process. The core of cobalt ferrite nanoparticles was prepared by successive sol-gel methodology, while the carbon-coated materials were obtained through the polymerization of tetraethyl orthosilicate (TEOS), resorcinol-formaldehyde (RF) and phloroglucinol- glyoxylic acid (PG). Subsequently, the materials were submitted to carbonisation under an inert atmosphere of N2 at temperatures of 120 and 400 °C for 1 h for each temperature and 600 °C for 3h. Subsequently, the subsequent removal of silica via washing with NaOH for 16 h. The adsorption isotherms obtained were classified as type IV, typical of materials with mesoporous structure. After the preparation and characterization of the materials, the synthesized catalysts were tested for the removal of paracetamol by wet catalysis with hydrogen peroxide under operating conditions of 80 °C, $C_{PCM,0}$ = 100 ppm, $C_{H202,0}$ = 472 mg/L, pH0 = 3.5 and $C_{catalyst}$ = 2.5 g L^{-1}, in which over 24 h the concentrations of PCM, H2O2 and aromatic compounds were monitored. All catalysts showed catalytic activity for the removal of PCM by CWPO, in which 100% of PCM removal was obtained for all catalysts after 24 h of reaction time. However, different H_2O_2 decomposition and PCM removal profiles were observed for the uncoated and coated nanomaterials. Both the carbon-coated catalysts outperformed the results obtained for the uncoated catalyst in terms of H_2O_2 and PCM decomposition. For the coated materials complete decomposition of PCM was obtained within 6 h of reaction time, while in the same time interval using the uncoated material as a catalyst, only 47% of the initial amount of PCM was degraded from the system. The catalyst coated by the greener method ($CoFe_2O_4$@PG) showed a profile of higher selectivity in hydrogen peroxide decomposition and a higher decrease in concentration of aromatic compounds throughout the reaction time. The coated materials were reused in oxidation tests, in which they presented a lower amount of leached iron as well as an increase in catalytic activity, leading to the complete degradation of paracetamol in 4 h of reaction.

Keywords: Magnetic nanoparticles; Paracetamol; Advanced oxidation processes; Carbon-based materials.

RESUMO

Este trabalho aborda o revestimento de carbono de nanopartículas magnéticas baseadas em ferritas de cobalto ($CoFe_2O_4$) através de um método tradicional ($CoFe_2O_4$@RF), um método mais verde ($CoFe_2O_4$@PG) e sua posterior funcionalização no processo CWPO. O núcleo das nanopartículas de ferritas de cobalto foi preparado por metodologia sucessiva de sol-gel, enquanto os materiais revestidos de carbono foram obtidos através da polimerização do tetraethyl orthosilicate (TEOS), resorcinol-formaldeído (RF) e phloroglucinol-ácido glioxílico (PG). Posteriormente, os materiais foram submetidos a carbonização sob uma atmosfera inerte de N_2 nas temperaturas de 120 e 400 °C por 1 h para cada temperatura e 600 °C por 3h. Em sequência, a posterior remoção da sílica via lavagem com NaOH por 16 h. As isotermas de adsorção obtidas foram classificadas como tipo IV, típica de materiais com estrutura mesoporosa. Após a preparação e caracterização dos materiais, os catalisadores sintetizados foram testados para a remoção do paracetamol por meio da catálise húmida com peróxido de hidrogênio sob condições de operação de 80 °C, $C_{PCM,0}$ = 100 ppm, $C_{H2O2,0}$ = 472 mg/L, pH_0 = 3.5 and $C_{catalyst}$ = 2.5 g L^{-1}, no qual ao longo de 24 h foram monitoradas as concentrações de PCM, H_2O_2 e compostos aromáticos. Todos os catalisadores mostraram atividade catalítica para a remoção do PCM por CWPO, no qual 100% de remoção do PCM foi obtida para todos os catalisadores após 24 h de tempo de reação. Entretanto, foram observados diferentes perfis de decomposição de H_2O_2 e remoção de PCM para os nanomateriais não revestidos e revestidos. Ambos os catalisadores com revestimento de carbono superaram os resultados obtidos para o catalisador não revestido em termos de decomposição de H_2O_2 e de PCM. Para os materiais com revestimento foi obtido a decomposição completa do PCM dentro de 6 h de tempo de reação, enquanto no mesmo intervalo de tempo utilizando o material não revestido como catalisador, apenas 47% da quantidade inicial de PCM foi degradada do sistema. O catalisador revestido pelo método mais verde ($CoFe_2O_4$@PG) apresentou um perfil de maior seletividade na decomposição de peróxido de hidrogênio e um maior decréscimo de concentração de compostos aromáticos durante todo o tempo de reação. Os materiais revestidos foram reutilizados em testes de oxidação, no qual apresentaram uma menor quantidade de ferro lixiviado bem como um aumento de atividade catalítica, levando a degradação completa do paracetamol em 4 h de reação.

Palavras-chave: Nanopartículas magnéticas; Paracetamol; Processos oxidativos avançados; Revestimento de carbono.

TABLE OF CONTENTS

LIST OF ACRONYMS

WWTPs	- Wastewater treatment plants
AOPs	- Advanced oxidation processes
CWPO	- Catalytic wet peroxide oxidation
MNPs	- Magnetic nanoparticles
NCs	- Nanocomposites
CSNPs	- Core-shell nanoparticles
HCSNPs	- Hollow core-shell nanoparticles
MRI	- Magnetic Resonance Imaging
CAs	- Contrast agents
GD	- Gadolinium
IONPs	- Iron oxide nanoparticles
NP	- Nanoparticle
PGA	- Phloroglucinol/glyoxylic acid
WAO	- Wet air oxidation
HPLC	- High pressure liquid chromatography
PCM	- Paracetamol
H_2O_2	- Hydrogen peroxide
Cat	- Catalyst
T	- Temperature
TEOS	- Tetraethyl orthosilicate
CEC	- Contaminants of emerging concern

LIST OF FIGURES

LIST OF TABLES

1 INTRODUCTION

Water is a vital and limited resource for all life on earth and particularly precious for human civilization. One of the sustainable development goals for the 21st century is to provide clean and affordable water for everyone [1]. However, factors such as industrialization, urbanization and water misuse lead to contamination and wastes. Most wastewaters are discharged directly into the environment without adequate treatment, generating impacts on human health, on economic productivity, on the quality of freshwater resources and on ecosystems [1,2]. The pollution of the aquatic environment arises from the various types of contaminants of emerging concern (CEC) that may be present in this environment [3,4]. The accumulation of these compounds in water resources can lead to the development of microorganisms resistant to antibiotics, affecting humans directly and indirectly [5].

Micropollutants are a wide range of substances that can be originated naturally or from anthropogenic activities, such as pharmaceutical compounds, steroid hormones and agrochemicals [3]. Several studies have reported the occurrence of pharmaceutical compounds in the environment, mainly in water since the conventional water treatment methods do not impede them to infiltrate the water cycle, reaching humans [4,6]. Since a large proportion of these pharmaceutical compounds cannot be metabolized and assimilated by the human body, this source of pollutants arises directly from the excretion of urine or faeces after drug administration to humans and animals in hospitals, households and farms [4,7].

Generally, micropollutants are not found individually in water resources. As a result, this mixture of micropollutants may have a synergistic effect, making it more difficult to detect, quantify and remove [3]. Therefore, it is extremely important to develop and improve efficient treatments technologies to remove those pollutants from wastewater. Among those technologies it is possible to highlight advanced oxidation processes, which represents a set of methodologies based on the formation of hydroxyl radicals for the oxidation of organic micropollutants [7]. In this sense, among AOPs, catalytic wet peroxide oxidation (CWPO) has proved to be an efficient technique to remove micropollutants using suitable catalysts.

1.1 Objectives

The main objectives of this dissertation consist in the functionalization of magnetic nanoparticles (MNPs) coated with carbon materials, in which friendly environmental components such as Pluronic F-127, Glyoxylic Acid and Phloroglucinol are used as precursors of carbon polymeric resin, as alternative to noxious formaldehyde-based resins. The developed MNPs are subsequently applied as catalysts in the CWPO for paracetamol removal.

STATE OF THE ART

2 STATE OF THE ART

2.1 Magnetic nanoparticles

Over the last 10 years researchers have shown an increased interest in MNPs. Analysing the statistics at the Scopus database of the publications about MNPs since 2011, more than 80.909 papers have been published, as shown in Figure 1 (a). In addition, to the Web of Science database, the number of documents published per year has been linearly increasing, reaching 93.528 for the same period analysed previously, Figure 1 (b). By means of the analysed data it is possible to visualize that the studied topic is of extreme interest in the scientific community, since the number of publications is increasing over the years, due to the various applications of this type of material.

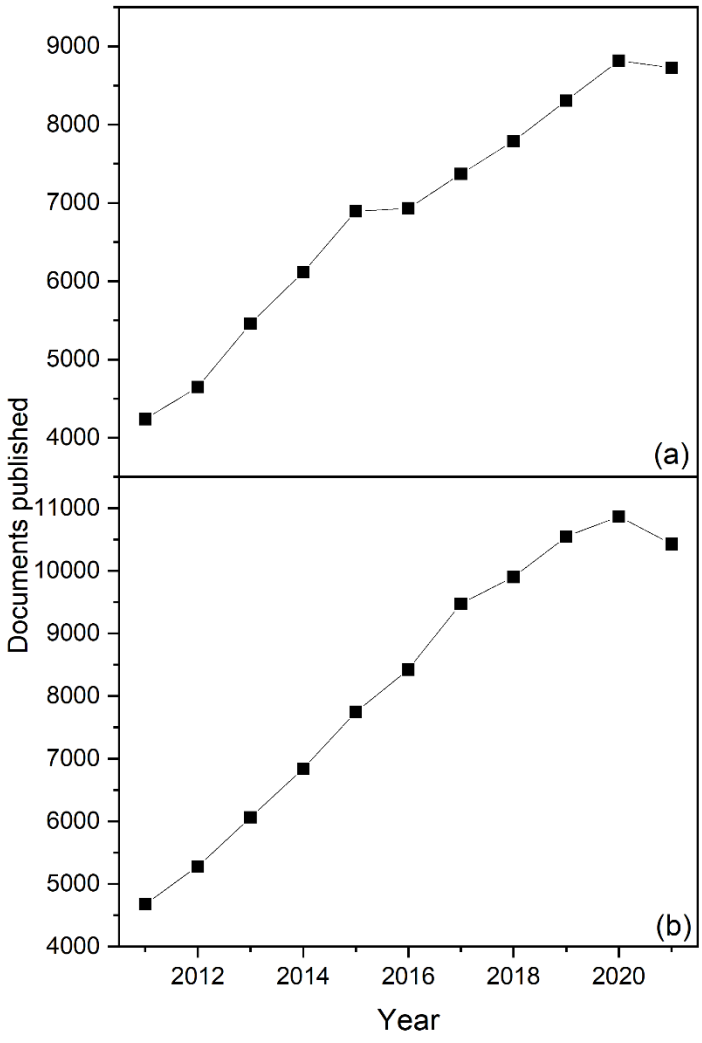

Figure 1 - Documents published per year during the last decade.
Source: (a) Scopus and (b) Web of Knowledge (keyword: Magnetic nanoparticle).

MNPs are typically defined as materials with at least one dimension smaller than 100 nm. Those materials present different properties such as a high surface-area-to-volume ratio, high reactivity for contaminant removal and strong sorption when compared to the bulky state. These differences can be explained due to the greater manifestation of quantum effects at the nanometre scale, in which physical and chemical properties depend on size, morphology and crystalline structure [8,9].

During the last decade, MNPs have been the focus of attention in the scientific and industrial community due to their wide range of applications, such as magnetic energy storage, catalysis, environmental remediation, magnetic inks and magnetic resonance imaging (MRI) [10]. Besides, due to their intrinsic magnetic properties, they can be simply manipulated using an alternating magnetic field, allowing to synthesize MNPs with specific morphology and surface area, manipulating their characteristics for different sorts of applications [11].

Various metals can be used to build the core of a magnetic nanoparticle. The choice of metal is related to its economic value, resource availability and its physical, chemical and magnetic properties [11,12]. Several pure phases of iron oxides are found in nature, the most popular MNPs being iron-based, namely zero-valent iron (nZVI), (Fe_3O_4 and Fe_2O_3). They possess different physical and chemical properties originated from the difference in their iron oxidation states and their capability for contaminant removal. Magnetite (Fe_3O_4), a ferromagnetic black coloured iron oxide of both Fe(II) and Fe(III), has been widely studied due to the presence of the Fe^{2+} state with the potential of acting as an electron donor [13,14].

2.2 Applications of MNPs

MNPs are superparamagnetic because of their nanoscale size, offering great potentials in a variety of applications in their bare form or coated with a surface coating and functional groups chosen for specific uses. Several applications of MNPs have been reported, such as, drug delivery, magnetic resonance imaging (MRI), catalysis, among others. [15,16]

2.2.1 Drug Delivery

One of the possible applications of MNPs is in drug delivery as drug nanocarriers. The drug delivery process consists of the addition of MNPs in which the drugs will attach and guide those nanoparticles to a specific region of the body by the action of magnetic

field gradients, keeping the particles in this region until the end of therapy, followed by their removal. Among the main advantages of using MNPs as loading agents can be highlighted their potential to load high doses of drugs, to raise the concentration of this drug in a specific site, avoiding toxicity and possible collateral effects of high concentrations of drugs in other parts of the body [15]. Furthermore, their ability to convert magnetism into heat represents one opportunity of synergistic cancer therapy, eliminating cancer cells also by hyperthermia [17].

There are some characteristics necessary to ensure that nanoparticles can stay for a long time in circulation executing drug delivery, such as surface chemistry, structure and size [18]. It is believed that MNPs with sizes ranging from 10 to 100 nm are most suitable for drug delivery applications [15]. The lower threshold is based on the fact that particles smaller than 10 nm are easily removed by extravasation and renal clearance. The upper threshold is not well defined. However, some recent data suggest that nanoparticles in the range 50–100 nm are smaller than the spleen cut off (200 nm) and can penetrate large tumors following systemic administration [15].

2.2.2 Magnetic Resonance Imaging (MRI)

MNPs have been investigated as contrast agents in MRI for many applications such as cell labelling, tumour imaging and tissue engineering. In the medical field, MRI can provide both anatomical and functional information, with excellent image quality, using non-ionizing radiation, allowing studies to be performed without the risk of side effects [19,20].

Gadolinium (Gd) is the most common contrast agent (CA) used in clinical practice to enhance image contrast. However, CAs lack specificity and have recently been related to toxicity issues caused by the unexpected release of free Gd. From that, magnetic nanoparticles have arisen as a promising alternative with improved properties in terms of specificity and biocompatibility [19].

Over the last years, several studies aimed at the development and improvement of new magnetic materials for medicinal applications. Among the materials developed, iron oxide nanoparticles (IONPs) have been widely investigated as a contrast agent in magnetic resonance imaging due to their magnetic property of superparamagnetism, high biocompatibility, low toxicity and easiness of functionalization of their surfaces with target molecules for molecular imaging purposes [20].

2.2.3 Catalysis

The use of MNPs in catalytic processes has been widely investigated owing to the significant improvements in catalytic performance when compared to traditional heterogeneous catalysts [12,21]. The increased performance when using MNPs is attributed to the large surface areas and to the high number of surface atoms, leading to many active sites. Besides, it is important to highlight that catalytic properties can be influenced by nanoparticle size, shape and capping molecules on the surface [22].

The nanomaterials in the reaction medium can act as nanoreactors, which are defined as chemical reaction receptor nanospheres that contain a catalyst within their boundaries. Nanoreactors are becoming increasingly used owing to their ability to hold reagents and catalysts for a long period and their ability to protect catalysts from environment influences. In general, these materials must present a few characteristics such as fast diffusion of reactants, a suitable structure to protect the catalytic species and long-term stability [23,24].

Three factors are of particular importance for nanoparticle catalysis. One is the sustainability of the metal incorporated into the nanoparticle (NP), since many metals are becoming scarce. Two other factors, which concern sustainability in NP catalysis, are consideration of PBT (persistence, bioaccumulation and toxicity) [25] for both substrates (as well as products) and solvents. If any substrate is environmentally risky, a new process that involves safe starting materials and intermediates should be used [26].

2.3 Structure of Nanomaterials

Core-shell, hollow core-shell and rattle core-shell nanostructures (yolk-shell) are among the main structures of NPs studied nowadays. Figure 2 shows those types of structures [18,23].

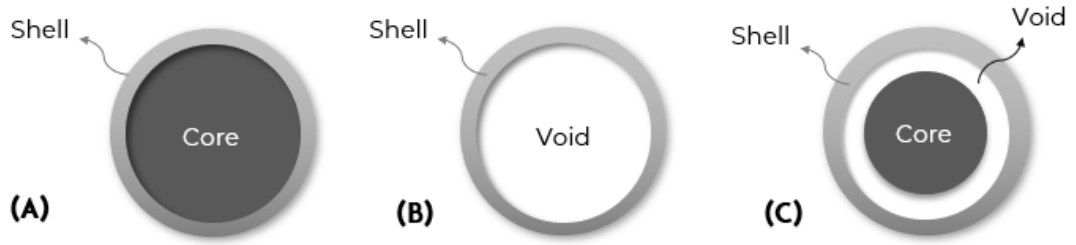

Figure 2 - Multifunction nanomaterials including (a) core-shell, (b) hollow core-shell and (c) yolk-shell. (Adapted from Figure 1 of [20])

Coating nanoparticles with one or more layers of materials that have interesting properties has been widely used by scientists for protection and performance enhancement. The original nanoparticle, named core, is encapsulated by a layer named shell and, due to this added layer, the core can exhibit a new catalytic activity resulting from the synergistic effect between the core and the shell. It is important to highlight that the addition of more than one shell to the newly formed structure can present different functionalities when compared with the core by itself, thus offering a wider range of applications in different areas [23,27].

There are a variety of components that can be used to build a core, such as metals (Au, Cu, Pt, Ni, Pd), oxides (SiO_2, Fe_2O_3, Fe_3O_4, Co_3O_4), doped oxides ($Gd_2O_3:Eu^{3+}$), whereas the shell can be made of metal (Pt), oxides (SiO_2, $CuSiO_3$, Fe_2O_3, SnO_2), polymers or carbon. The choice of metals, oxides or polymers for the formation of the core and shell varies according to the purpose of its application. Generally, the functionality of the nanoparticle depends on the composition of the core, while the shell has the function of protection and transport of substances due to its porous surface [18].

2.3.1 Core-Shell

Core-shell nanoparticles (CSNPs) are materials that present in their structure an active core coated by one or more layers of different materials. The properties and functionalities of CSNPs depend mainly on two factors, the choice and combination of the materials that compose their structure and the final particle size [28]. The selection of a suitable core size is crucial to design an efficient core–shell system.

Regarding the synthesis of CSNPs, two techniques have been widely used by the scientific community, which are “top-down” and “bottom-up”. The “top-down” approach uses external controls such as microfabrication techniques and mechanical stress to broke

down the bulk materials into smaller ones to obtain different shapes and sizes of NPs. Whereas the "bottom-up" technique is used to synthesize CSNPs from molecular or atomic building blocks. Control of shape and size of NPs will be achieved through the inherent chemical properties of each of the constituents and the mutual interactions between them [28]..

2.3.2 Hollow Core-Shell

The main structural difference between hollow core-shell nanoparticles (HCSNPs) and CSNPs corresponds to the absence of core in their structure. The development of HCSNPs arose because of geometric modifications made in the structure of NPs to obtain more flexibility and storage capacity. Due to the absence of core, the particle presents unique properties such as uniform size, well-defined morphology, high surface area and low density [23].

The absence of core and the large fraction of empty space in the structure of HCSNPs are responsible for promoting numerous applications. As an example, hollow structures have been used in the loading and controlled release of specific molecules, such as drugs, peptides and genes [29]. In addition, the hollow space of the sphere can also be used as a nanoreactor for catalytically active particles and provide labelled images for detection of cancer and other diseases [23].

2.3.3 Yolk-Shell

Yolk-shell nanoparticles (YSNPs) represent a new class of materials, generally denoted by core-void-shell or core@void@shell, which present tailored physical and chemical properties. The tailor-ability and functionality of both configurations make yolk-shell structures able to have several applications in different fields, such as catalysis, biosensors, storage capacity and transport of substances [23,30].

YSNPs have emerged through the need to combine the functionalities present in the structure of CSNPs, such as the synergistic effect between core and shell, and the empty space present in hollow structures. Thus, YSNPs are defined as hybrid structures (mixture of core/shell and hollow) where a core particle is encapsulated inside the hollow shell and may move freely inside the shell [18,31].

Several synthetic methods for the preparation of YSNPs, such as selective etching, hard template and soft templating have been developed to obtain specific compositions,

architectures and dimensions [26]. Selective etching uses chemical treatments or calcination to selectively remove either part of the shell or part of the core to create a void between both structures. Generally, the void is created by addition of a basic etchant (such as NaOH) to etch out core of shell material [32]. Hard-template approach consists of the use of a pre-synthesised metal core coated with an inert template (as silica or zeolite). Thereafter this structure is infiltrated with a carbon precursor followed by a carbonization and further removal of the template by acid or basic washing [26,32].

Soft-template approach consists of the self-assembling of carbon precursors with a soft block copolymer via hydrogen bonding, followed by a thermopolymerization and carbonization of the structure, resulting in obtaining magnetic nanoparticles coated by a carbon layer [33]. The shell thickness and core size can be adjusted according to the amount of reactant added during the catalyst synthesis and carbon-coating methodology [18].

For a catalyst to be considered good it must follow some characteristics, such as long life of use, reusability, catalytic activity, selectivity and stability, even in harsh conditions [34]. Due to the structure of yolk-shell nanoparticles, the active site for the catalytic reaction is protected by a shell, which prevents the degradation of the nanoparticle during the catalytic reaction. Moreover, the shells of YSNPs are porous and permeable, allowing diffusion of reactants in and out of the YSNPs through the nanoporous channels, while protecting the metal core from sintering and aggregation [18,26].

2.4 Environmentally precursors of carbon

The carbon polymer resin that gives rise to the carbon shell that will coat the core can be synthesised from different methodologies such as hard-template and soft-template. In the hard-template approach, an inert template (as silica or zeolite) is infiltrated with a carbon precursor followed by a carbonization and further removal of the template by acid or basic washing. However, this approach has some disadvantages such as the removal of the template in harsh acidic or basic conditions, several steps, and the use of toxic reagents such as resorcinol and formaldehyde as precursors of the polymeric carbon resin [35].

The most employed phenolic compounds are phenol, resorcinol and phloroglucinol, and formaldehyde used as a cross-linker. Formaldehyde is a carcinogen component, which represents an important drawback for the process. To surpass these

drawbacks, novel friendly environmental materials such as, phloroglucinol and glyoxylic acid represents an alternative carbon precursors over the traditional reactants resorcinol-formaldehyde [35].

Glyoxylic acid has attracted a lot of attention, since its bi-functionality (aldehyde and carboxylic acid groups) plays a double role in carbon synthesis, as a cross-linker for the formation of the phenolic resin and as a catalyst, as it can promote polymerization of the phenolic resin [33]. Besides, phloroglucinol was found to react with glyoxal and triblock polymers, such as Pluronic F-127, in a similar way to resorcinol-formaldehyde [36,37]. In addition, glyoxylic acid is found in plants and its release into water, air and soil is harmless, due to its biodegradable nature. Therefore, the use of these reagents to produce carbon structures becomes advantageous due to the environmental properties of the reagents [33].

2.5 Advanced Oxidation Process

Wastewater treatment plants (WWTPs) might minimize the discharge of micropollutants into receiving waters and still improve the overall secondary effluent quality status for possible reuse [38]. However, the conventional biological treatment in WWTPs is not able to degrade persistent organic pollutants such as endocrine-disrupting compounds, many sorts of pharmaceutical drugs, including antibiotics, pesticides and surfactants, among others [39].

The upgrading of WWTPs by the implementation of additional advanced processes such as AOPs, before discharge into the environment, has arisen as practice for the total mineralization of micropollutants, or by converting them into less harmful compounds [21,40].

AOPs are considered clean technologies for the treatment of polluted waters that apply the concept of producing hydroxyl radicals ($HO^{\bullet}$), which will degrade the organic pollutants [21,40]. Hydroxyl radical constitutes one of the most powerful oxidants (E^0 = 2.73 V), much stronger than other conventional oxidizing species such as hydrogen peroxide (E^0 = 1.31 V) or ozone (E^0 = 1.52 V) [21,41]. The highly oxidizing radicals will be responsible for the degradation of pollutants into CO_2, water and inorganic ions [42].

There are several technologies among AOPs that can be used for wastewater treatment, such as ozonation, photolysis, electrooxidation and Fenton [43].

Ozone is one of the highly oxidative agents for the oxidation of chemicals among pure oxygen and air [12]. The ozonation process in wastewater occurs through the decomposition of ozone to produce HO• radicals, initiating a chain reaction in which the radicals formed will be responsible for promoting the process (Equation (1) and (2)) [44]. Besides, the addition of hydrogen peroxide is responsible for increased ozone decomposition and, consequently, higher production of HO• radicals (Equations (2) and (3)) [12].

$$O_3 + OH^- \rightarrow HO_2^- + O_2 \quad (1)$$

$$HO_2^- + O_3 \rightarrow HO^\bullet + O_2^- + O_2 \quad (2)$$

$$H_2O_2 \rightarrow HO_2^- + H^+ \quad (3)$$

The use of ultraviolet radiation is another way to produce HO• radicals. A combination of UV radiation with wavelength lower than 280 nm results in the quick formation of OH• radicals (Equation (4)) by homolytic cleavage.

$$H_2O_2 + h\nu \rightarrow 2\ HO^\bullet \quad (4)$$

Some catalysts allow to use radiation with higher wavelength than 280 nm. The process is then known as photocatalysis. The combination of UV with other AOPs, including H_2O_2, not only increases the rate of HO• radical formation, but also reduces the process cost which is the main drawback of most AOPs [45].

2.5.1 Fenton Process

The Fenton process is one of the most studied among AOPs for the treatment of recalcitrant substances in wastewater [37,45]. The process uses Fenton reagents (H_2O_2 and ferrous iron) to produce HO• radicals. The interaction between H_2O_2 and Fe^{2+} results in the decomposition of H_2O_2 through the oxidation of Fe^{2+} to ferric ion Fe^{3+}, leading to the formation of HO• radicals, as described by (Equation (5)) [39]. Subsequently, these ferric ions formed react with hydrogen peroxide producing hydroperoxyl radicals and regenerating the catalyst, the ferrous ions. (Equation (6)) [21].

$$H_2O_2 + Fe^{2+} \rightarrow OH^- + HO^\bullet + Fe^{3+} \quad (5)$$

$$Fe^{3+} + H_2O_2 \rightarrow Fe^{2+} + HOO^\bullet + H^+ \quad (6)$$

During the oxidation of the organic pollutants, intermediates species are formed. In sequence, these intermediates are oxidised up to CO_2, H_2O, inorganic salts and other substances, depending on the presence of heteroatoms in the organic matter contained in the wastewater. Thus, the overall process can be schematically described by Equations 7 and 8 [46].

$$\text{Pollutants} + H_2O_2 \rightarrow \text{intermediates} \quad (7)$$

$$\text{intermediates} + H_2O_2 \rightarrow CO_2 + H_2O + \text{inorganic salts} \quad (8)$$

Among the advantages of using the Fenton process for wastewater treatment, it is possible to highlight the simplicity of the equipment used and the mild operating conditions usually employed. In addition, hydrogen peroxide is safe and easy to handle and no after-treatment is necessary due to its decomposition into water and oxygen [46].

Factors such as the concentration of H_2O_2 need to be extremely precise to ensure the efficiency of the process, since high concentrations of H_2O_2 can lead to radical scavenger reactions (Equation (9) and (10)) [37,47]. The hydroperoxyl radicals ($HOO^{\bullet}$) formed are much less reactive and do not significantly contribute to the oxidative degradation of organic substrates, which mainly occur by reaction with $HO^{\bullet}$ [47].

$$H_2O_2 + HO^{\bullet} \rightarrow HOO^{\bullet} + H_2O \quad (9)$$

$$HOO^{\bullet} + HO^{\bullet} \rightarrow O_2 + H_2O \quad (10)$$

Although the Fenton process is effective for many wastewater treatments, it has some disadvantages such as high operation cost, limited optimum pH range, large volume of sludge produced and difficulties in recycling the homogeneous catalyst (Fe^{2+}) [37,48]. In this context, the use of a solid catalyst in a heterogeneous Fenton-like oxidation, also known as catalytic wet peroxide oxidation, is a promising alternative.

2.5.2 Catalytic wet peroxide oxidation

Catalytic wet peroxide oxidation (CWPO) consists in the use of a solid catalyst to decompose hydrogen peroxide into $HO^{\bullet}$ radicals to oxidize non-biodegradable substances [6,39]. CWPO is considered to be a low-cost technology because it can be operated without lamps and at mild operation conditions [1].

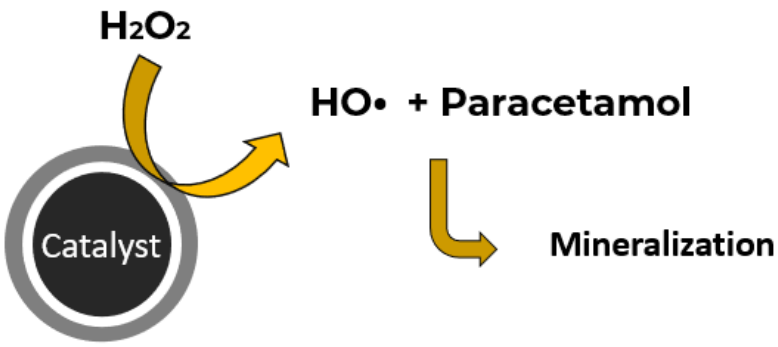

Figure 3 - Decomposition of hydrogen peroxide into hydroxyl radicals.

The organic pollutants that are present in wastewaters are degraded by hydroxyl radicals ($HO^{\bullet}$) generated due to the partial decomposition of H_2O_2, promoting, with an appropriate catalyst, the non-selective degradation caused by $HO^{\bullet}$ radicals to treat a wide range of industrial wastewaters, including pharmaceutical wastewaters [6].

Among the catalysts used in CWPO, iron-based materials have been attracted the attention of scientists. Those materials can initiate a Fenton process over solid surfaces by heterogeneously catalysing the degradation of organic compounds. During the process, hydrogen peroxide (H_2O_2) is decomposed into $HO^{\bullet}$ and the radicals react with organic compounds along with their intermediates. Some metals with multiple redox states can also work as Fenton catalysts with similar catalytic mechanisms to those with iron-based catalysts, such as Mn, Co, Cu and Ce [49,50].

In order to promote improvements in the catalytic process, the use of supported catalysts has been widely explored, as it allows increasing the surface area of the metal species by providing a matrix that enables their dispersion as very small particles [51]. The high metal dispersion diminishes the sintering of the active phase, improves the thermal and chemical stability of the catalyst and avoids the continuous loss of catalyst [46,52]. However, the leaching of metal active phases is usually observed depending on the operating conditions [53]. For this reason, novel approaches proposed the use of encapsulated iron-based catalysts (e.g. YSNPs), promoting the diffusion of the pollutants inside the nanoparticle, but avoiding the leaching of the metal contained within the shell [39].

Characteristics such as stability, reusability and recovery represent a key issue regarding its potential application [38]. CWPO is usually carried out with the catalyst in

the form of suspended powdered particles, then requiring further separation to recover the material from the reaction medium [21]. Thus, as a way to improve the separation process, the development of magnetic catalysts provides an interesting solution, allowing easy, fast and inexpensive separation upon the application of a magnetic field, simplifying its recovery and reusability [21]. Figure 4 represents schematically the steps of application and reusability of $CoFe_2O_4$.

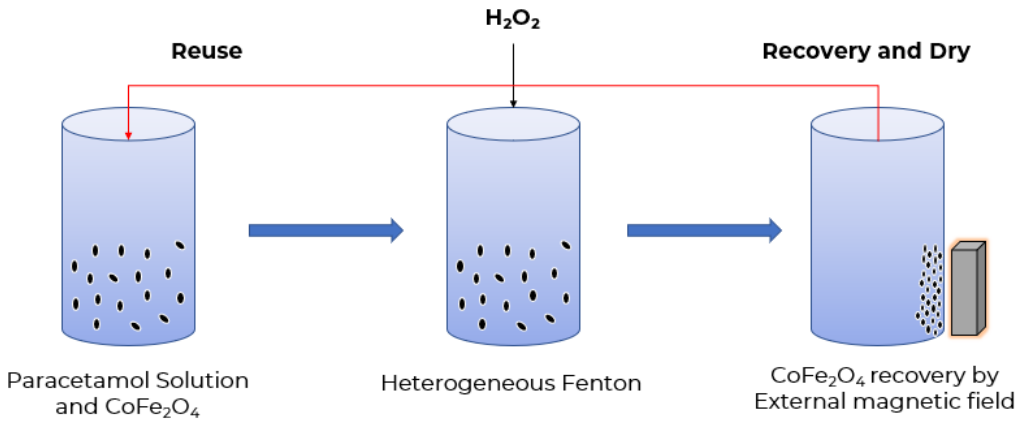

Figure 4 - Illustration of the application process and reuse of the catalyst ($CoFe_2O_4$).

The main parameters that influence the heterogeneous Fenton process are the initial solution pH, the reaction time, temperature, catalyst and oxidant dosages [21]. Table 1 shows some magnetic nanoparticle structures used for the degradation of several types of pollutants, as well as their reaction conditions.

The initial solution pH can significantly affect the degradation of many pollutants. Do et al. [54] have analysed the decomposition of acetaminophen (ACTM) using the magnetic yolk-shell Fe_3O_4@SiO_2@Cu and the better catalytic activities were observed at pH 3.0. Also, it was observed that the ACTM removal efficiency decreased as pH increased, which can be explained by the formation of a weaker oxidant and lower generation of $HO^{\bullet}$ radicals at higher pH values.

Do et al. [54] have also analysed the effect of H_2O_2 concentration on the removal of ACTM using a yolk shell nanoparticle as catalyst. It was observed that degradation of ACTM was enhanced with the increase of H_2O_2 concentration. This enhancement was attributed to the accelerated generation of reactive species when higher amounts of H_2O_2 were added [54,55]. However, the degradation efficiency decreases with a higher dosage

of H_2O_2, since high concentrations of H_2O_2 can lead to the formation of hydroperoxyl radicals, which have significantly lower oxidative ability [37].

Catalyst dosage plays an important role in CWPO processes, since the participation of higher quantity of catalyst can accelerate the degradation of organic compounds. In the heterogeneous Fenton process, the reaction between ferrous or ferric ions and hydrogen peroxide takes place at the surface of the solid catalyst and then depends on the specific surface area of the catalyst [56,57]. Do et al. [54] have analysed the effect of catalyst dosage on the removal of ACTM from 0.02 to 0.20 g/L for a magnetic yolk-shell Fe_3O_4@SiO_2@Cu and, as a result, observed that the increase of catalyst dosage led to an increase in the number of actives species, which favoured hydrogen peroxide decomposition and, consequently, higher formation of hydroxyl radicals $HO^{\bullet}$.

The reaction parameters for CWPO vary according to the type of pollutant in which the degradation is desired. The typical operating conditions are initial pH 2 to 7; 25 to 160 °C; 1 to 10 bar; 0.2 to 10 g L^{-1} catalyst concentration; and a dose of H_2O_2 from 50 to 200 % of the stoichiometric quantity needed to mineralize the organic matter contained in wastewaters [1,21,39].

Table 1 - Scope of magnetic nanoparticles in CWPO processes.

Catalyst	Model pollutant	Operating CWPO process	Best measured result	Reference
Cobalt ferrite encapsulated in graphitic shell ($CoFe_2O_4$/MGNC) (D: 7 nm)	4-nitrophenol (4-NP) $C_{(4-NP)} = 5.0$ g L^{-1}	pH_0 = 3.0 $C_{cat} = 5.0$ g L^{-1} $C_{H2O2} = 17.8$ g L^{-1} Reaction time = 4 h Temperature = 40 °C	$X_{TOC} = 79$ % $X_{4-NP} = 81{,}3$ % Leached Fe = 1.1 mg L^{-1}	[58]
Nickel Ferrite $FeNi_3$@SiO_2 (D: 40 – 70 nm)	Tetratetracycline (TC) $C_{TC} = 10 - 30$ g L^{-1}	pH_0 = 3.0 – 9.0 $C_{H2O2} = 150$ mg L^{-1} $C_{cat} = 0.005 - 0.1$ g L^{-1} Temperature = 20 °C Reaction time = 3 h	$X_{TC} = 87.27$ %	[59]
Magnetic/multi-walled carbon nanotubes (Fe_3O_4/MWCNTS) (D:<50 nm)	Naproxen (NP) $C_{NP} = 10$ mg L^{-1}	$pH_0 = 5.0 - 9.0$ Temperature = 30 – 70 °C $C_{cat} = 1.0$ g L^{-1} $C_{H2O2} = 0.5 - 2.5$ mM Reaction time = 3 h	$X_{TOC} = 50$ % $X_{NP} = 82$ %	[60]
Fe-Cu Doped Multiwalled Carbon Nanotubes Fe-Cu/CNT (D: 13.3 nm)	Paracetamol (PCM) $C_{PCM} = 50$ mg L^{-1}	$pH_0 = 6.3 - 6.6$ $C_{H2O2} = 13.8 * 10^{-3}$ mol L^{-1} $C_{cat} = 50$ mg L^{-1} Temperature = 25 °C Reaction time = 5 h	$X_{TOC} = 85.6$ % $X_{NPCM} = 98$ % Leaching of Fe = 3.99 mg L^{-1}	[61]

Table 1(continued)

Catalyst	Model pollutant	Operating CWPO process	Best measured result	Reference
Magnetic core-shell structured Fe_3O_4@CeO_2 (Size: 100-150 nm)	Benzoic acid (BA) $C_{BA} = 50$ mg L^{-1}	$pH = 3.2$ $C_{cat} = 1.0$ g L^{-1} $C_{H2O2} = 250$ mg L^{-1} Temperature = 30 °C Reaction time = 2 h	$X_{BA} = 80.0$ % $X_{TOC} = 48.0$ % Leaching of Fe = 4.2 mg L^{-1}	[49]
Yolk-shell structures for the removal of acetaminophen Fe_3O_4@SiO_2@Cu	Acetominophen (ACTM) $C_{ACTM} = 30$ mg L^{-1}	$pH = 5.0 – 7.0$ $C_{cat} = 0.02 - 0.2$ g L^{-1} $C_{H2O2} = 5.0 - 15.0$ mM Temperature = 25 °C Reaction time = 2 h	$X_{ACTM} = 100.0$ % Leaching of Fe = 0.02 mg L^{-1}	[54]
Alginate/Fe@Fe_3O_4 core/shell structured nanoparticles	Norfloraxin (NOF) $C_{NOF} = 50$ mg L^{-1}	pH = 3.5 C_{cat} = 0.4 g L^{-1} $C_{H2O2} = 0.98$ mM Reaction time = 1 h Temperature = 40 °C	$X_{NOF} = 100.0$ % $X_{TOC} = 90.0$ %	[62]
Nano-magnetite Nano-Fe_3O_4 (D = 30 nm)	Carbamazepine (CBZ) $C_{CBZ} = 15$ mg L^{-1} Ibuprofen (IBP) $C_{IBP} = 15$ mg L^{-1}	pH = 7.0 $C_{H2O2} = 600$ mM C_{cat} = 1.84 g L^{-1} Temperature = 23 °C Reaction time = 12 h	$X_{CBZ} = 90.0$ % $X_{IBP} = 81.1$ %	[63]

MATERIALS AND METHODS

3 MATERIALS AND METHODS

3.1 Reactants

The reactants used in this work are given below, separated by the application for which they were used.

3.1.1 Synthesis of the catalyst

- Ethanol (99.8%). Fisher Chemical; Formula: C_2H_6O.
- Ethanediol (99%). Fischer Chemical. Formula: $(CH_2OH)_2$
- Iron (III) chloride hexahydrate (99%). Aldrich. Formula: $FeCl_3.6H_2O$
- Cobalt (II) chloride hexahydrate (99%). Fischer Chemical. Formula: $CoCl_2.6H_2O$

3.1.2 Carbon-Coating

- Ethanol (99.8%). Fisher Chemical. Formula: C_2H_6O.
- Formaldehyde (38% w/w). Panreac. Formula: CH_2O.
- Resorcinol (99%). Alfa Aesar;Formula: $C_6H_6O_2$.
- Tetraethyl orthosilicate (TEOS) (98%). Fluka Chemika; Formula: $SiC_8H_{20}O_4$.
- Phloroglucinol dihydrate (98%). Alfa Aesar; Formula: $C_6H_3(OH)_3 \cdot 2H_2O$.
- Pluronic® F-127. Sigma Science.
- Sodium hydroxide (98%). Labkem; Formula: NaOH.
- Ammonia solution (28-30%). Merck; Formula: NH_3
- Glyoxal solution (40% w/w). Alfa Aesar; Formula: $C_2H_2O_2$
- Distilled Water

3.1.3 CWPO Runs

- Paracetamol (98%). Alfa Aesar; Formula: $C_8H_9NO_2$
- Hydrogen peroxide (30 % m/v). Fisher Chemical; Formula: H_2O_2
- Titanium (IV) oxysulfate (99.99%). Aldrich; Formula: $TiOSO_4$
- Sulfuric acid (98%). Labkem; Formula: H_2SO_4
- Sodium sulphite anhydrous (98%). Panreac; Formula: Na_2SO_3
- Ultrapure water

3.1.4 HPLC calibration curve

- Paracetamol (98%). Alfa Aesar; Formula: $C_8H_9NO_2$
- 4-Nitrophenol (99%). Acros Organics; Formula: $C_6H_5NO_3$
- Hydroquinone (99%). Merck KGaA; Formula: $C_6H_6O_2$
- *p*-Benzoquinone (98%). Alfa Aesar; Formula: $C_6H_4O_2$
- Resorcinol (99%). Alfa Aesar;Formula: $C_6H_6O_2$
- Phloroglucinol dihydrate (98%). Alfa Aesar; Formula: $C_6H_3(OH)_3 \cdot 2H_2O$.
- Catechol. Fisher Chemical; Formula: $C_6H_6O_2$
- Pyrogallol (98%). Alfa Aesar; Formula: $C_6H_6O_3$
- Acid ortho-phosphoric (85 %). Riedel-de Haen; Formula: H_3PO_4
- Acetonitrile (99,9%). Fischer Chemical; Formula: C_2H_3N
- Ultrapure Water

3.2 Synthesis of the magnetic catalyst

In the sol-gel method or sol-gel auto combustion, the chlorides/nitrates of the constituent metal ions and a suitable chelating agent (fuel), such as urea, glycine or ethylene glycol are used as the starting materials [64]. $CoFe_2O_4$ spinel ferrite nanoparticles were prepared by the sol-gel method using as precursors cobalt (II) chloride hexahydrate ($CoCl_2.6H_2O$) and iron (III) chloride hexahydrate ($FeCl_3.6H_2O$) in a ratio of 1:2.

The methodology of $CoFe_2O_4$ synthesis is described in literature [65], in which 2.38 g of $CoCl_2.6H_2O$ was weighed and dissolved in 10 mL of ethanol. This solution was stirred with a magnetic stirrer and heated until it reached the boiling point, approximately 78 °C. In the following, the cobalt solution was cooled down in an ice bath until thermal equilibrium at room temperature, 20 °C. Subsequently, 5.41 g of $FeCl_3.6H_2O$ was weighed and dissolved in 40 mL of ethylene glycol. This solution was heated with a magnetic stirring plate for 5 minutes at 60 °C. Soon after, the iron solution was cooled in an ice bath until thermal equilibrium was reached.

After thermal equilibration of both solutions, they were transferred to a single beaker. The resulting solution of the mixture was then kept in stirring with a magnetic stirrer at 60 °C for 2 h. Afterwards, the solution was heated to 189 °C until it turned to gel and subsequently, solid.

The solid material obtained after the combustion of cobalt ferrite precursors was further submitted to a thermal treatment in a furnace (Vertical tubular furnace ROS 50/250/12, Thermoconcept) under a temperature of 300 °C for 24 h and then at 600 °C for 12 h. The thermal treatment has been processed in an ambient atmosphere to remove possible organic impurities that were not degraded during the combustion, and to promote the crystallization of the material.

After the thermal treatment, the solid obtained was washed several times with distilled water and subsequently the solvent was changed from water to ethanol. Afterwards, the solid was dried in an oven under a temperature of 60 °C for 24 h. Figure 5 represents the steps related to the synthesis of the catalyst ($CoFe_2O_4$).

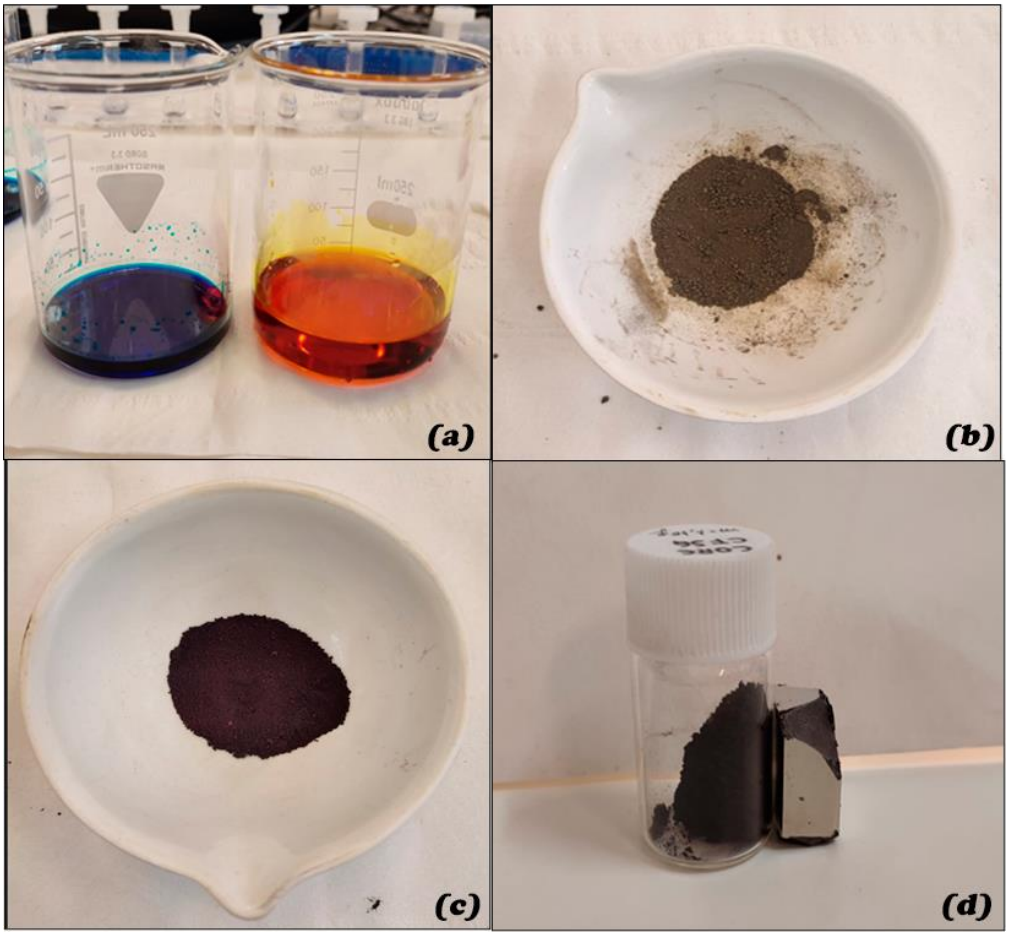

Figure 5 - (a) Solutions of: Cobalt (II) chloride hexahydrate and Iron (III) chloride hexahydrate; (b) Solid obtained after drying of the gel; (c) Solid obtained after thermal treatment and (d) Final solid obtained – $CoFe_2O_4$ (Bare Core).

3.3 Carbon-coating preparation

This section will discuss the steps of covering a magnetic nanoparticle spinel ferrite with a carbon layer. The steps are represented in Figure 6.

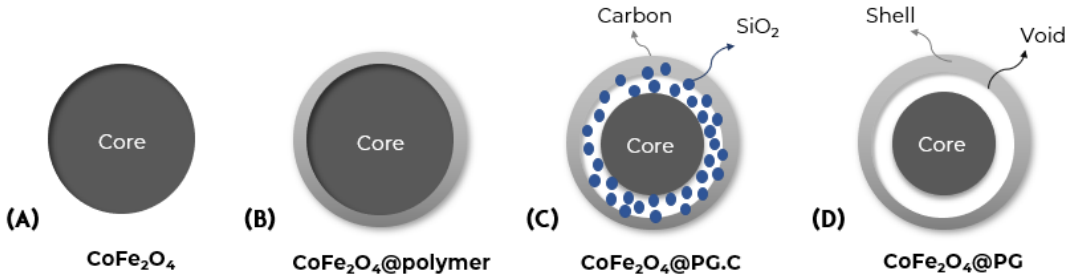

Figure 6 - Representation of the structures obtained at each step of the carbon-coating process.

3.3.1 Coating

The methodology used for the coating of the magnetic nanoparticles is illustrated in Figure 7.

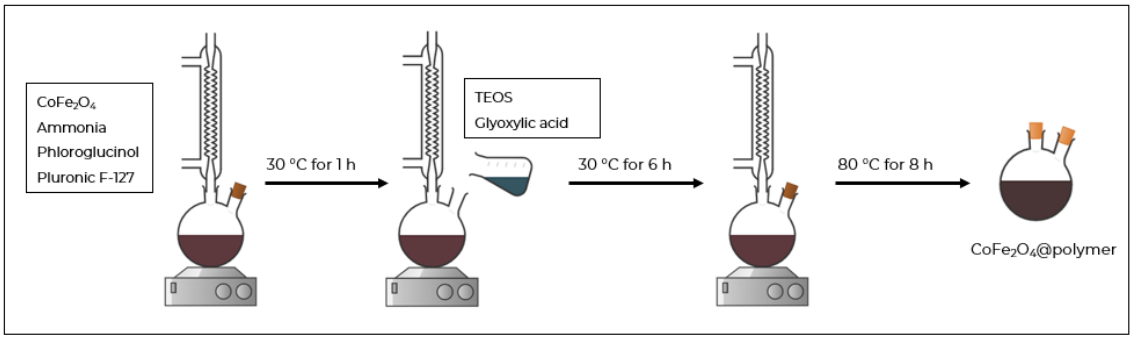

Figure 7 - Coating process of magnetic nanoparticles.

For the coating process, 0.25 g of $CoFe_2O_4$ nanoparticles were measured and added to a 250 mL Erlenmeyer flask containing 50 mL of distilled water. This solution was placed in an ultrasonic bath Ultrasons-H, P- Selecta, for 30 minutes at room temperature (20 °C), to obtain the dispersion of magnetic nanoparticles in the medium.

The dispersion was transferred to a 500 mL round bottom flask, which contained 0.10 g of Phloroglucinol, 0.20 g of Pluronic F-127, 1.2 mL of a 25% ammonia solution and 150 mL of absolute ethanol. The flask was placed in an oil bath and stirred with a magnetic stirrer at 30 °C for 1 h to mix the reagents. After 1 h, 0.21 mL of TEOS and 0.1 mL of glyoxylic acid were added into round bottom flask and the solution was kept stirred at 30 °C for 6 h. After 6 h at 30 °C, the temperature was increased, and the solution was

kept stirring at 80 °C for 8 h. The resultant solid obtained after the coating process was washed several times with distilled water until neutral pH, then with absolute ethanol and subsequently dried at 60 °C for 12 h in the oven. The resultant solid formed is denominated $CoFe_2O_4$@Polymer@PG

It was also obtained a solid material named $CoFe_2O_4$@Polymer@RF whose synthesis follows the same methodology for $CoFe_2O_4$@Polymer@PG. However, with the substitution of 0.10 g of Phloroglucinol, 0.20 g of Pluronic F-127 and 0.1 mL of glyoxylic acid for 0.10 g of Resorcinol and 0.15 mL of Formaldehyde.

3.3.2 Annealing

For annealing, the solid obtained was carbonized in a vertical tubular furnace (ROS 50/250/12, Thermoconcept) under a N_2 flow of (100 $Ncm^3.min^{-1}$). The thermal treatment of the gaseous phase was conducted at 120 °C (TSP_1) and 400 °C (TSP_2) during 1 h at each temperature and then at 600 °C (TSP_3) for 3 h using a heating rate of 120 °C/h ($RMP_{1,2,3}$). The operating conditions of the furnace are represented in Figure 8. The obtained magnetic nanoparticles after heat treatment were denoted $CoFe_2O_4$@PG.C and $CoFe_2O_4$@RF.C, according to the carbon precursors used during the synthesis.

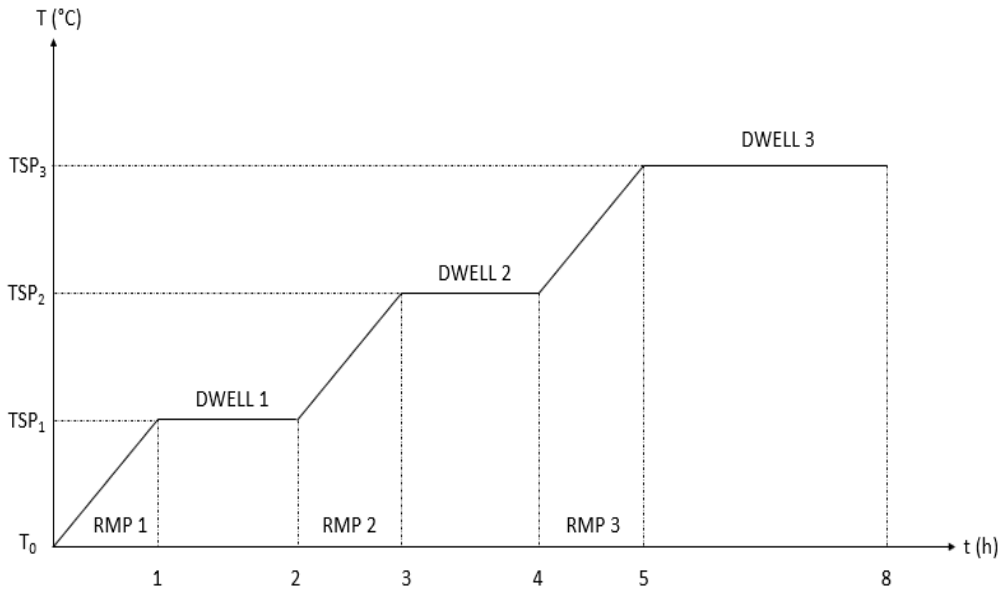

Figure 8 - Operation conditions of the furnace; TSP = Temperature of Set Point; RMP = Heating ramp; DWELL = Time taken at TSP.

3.3.3 Etching

The silica removal process was achieved by adding a NaOH solution (10 mol/L) at a ratio of 1 mL to every 10 mg of $CoFe_2O_4$@PG.C or $CoFe_2O_4$@RF.C in an Erlenmeyer flask. The solution formed was then stirred with a magnetic stirrer at room temperature for 16 h. The resultant material was washed several times with distilled water until neutral pH, then with absolute ethanol and subsequently dried at 60 °C for 12 h in the oven.

The catalysts used in this work are named $CoFe_2O_4$ (Bare Core), $CoFe_2O_4$@PG and $CoFe_2O_4$@RF. $CoFe_2O_4$@PG represents the catalyst obtained by an innovative methodology using greener carbon precursors (Phloroglucinol and Glyoxylic Acid) and $CoFe_2O_4$@RF represents the catalyst obtained following the traditional methodology, using Resorcinol-Formaldehyde as precursor reagents of the polymeric carbon layer.

3.4 Characterization of the materials

This session will present the methodologies used to characterise the catalysts used in the oxidation tests.

3.4.1 Surface and pore analysis

The textural properties of the materials were determined from N_2 adsorption-desorption isotherms at 77 K, obtained in a Quantachrome instrument NOVA TOUCH LX^4 adsorption-analyser, following the methodology described in previous group's work [66]. The process of degasification of the samples was performed at 120 °C during 16 h, followed by the measurement of the adsorption isotherms. The BET (Brunauer-Emmett-Teller) specific surface area (S_{BET}) was calculated in a range of p/p_0 0.05 – 0.35 and the total volume of pores was calculated considering p/p_0 0.98 [66]. All the calculations were performed using TouchWinTM software v1.21.

The BET method is one of the most widely used for the calculation of the surface area of porous materials. Usually, the BET equation is employed in the linear form, represented by Equation (11),

$$\frac{p/p^0}{n(1-p/p^0)} = \frac{1}{n_m C} + \frac{C-1}{n_m C}(p/p^0) \qquad (11)$$

where n is the specific amount adsorbed at the relative pressure p/p^0 and n_m is the specific monolayer capacity.

The total pore volume was obtained through Equation (12)

$$Total\ pore\ volume = \frac{n.M_{N_2}}{V_{N_2}.\rho} \quad (12)$$

Where M_{N_2} is the molar mass of N_2, V_{N_2} is the specific volume of N_2, and ρ is the density of N_2 (808000 $g\ m^{-3}$).

The International Union of Pure and Applied Chemistry (IUPAC) has published recommendations regarding physical adsorption characterization, including the classification of isotherms [67]. Figure 9 represents the classification proposed by IUPAC, which provides initial guidance on how to interpret adsorption isotherms for structural characterization.

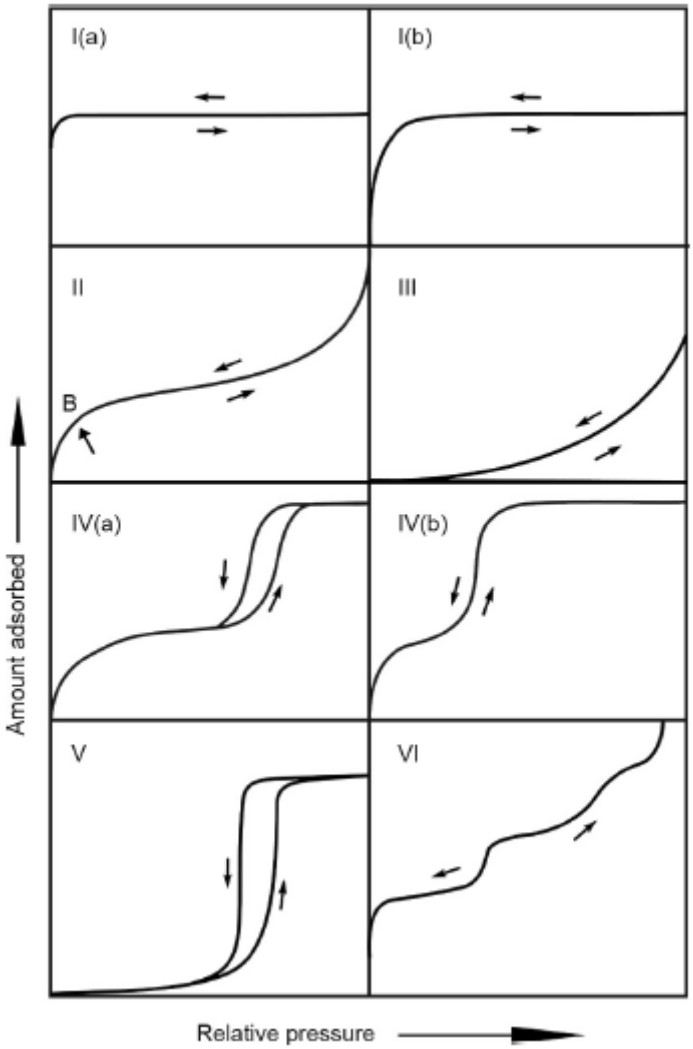

Figure 9 - Classification of physisorption [67]**.**

IUPAC also provide a classification of hysteresis loops, which occurs mainly due to the different pore sizes during the desorption. Figure 10 represents the hysteresis loops classification.

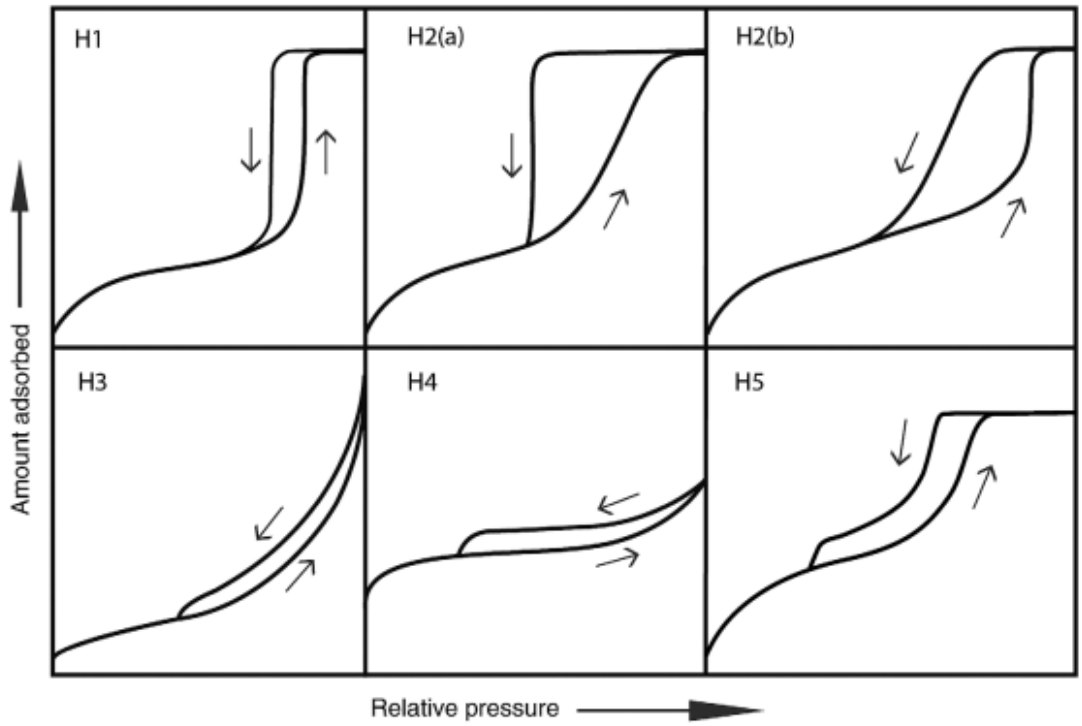

Figure 10 - Classification of hysteresis loops [67]**.**

3.4.2 Fourier Transform Infra-Red spectroscopy (FTIR) analysis

FTIR spectra of the 3 steps of carbon-coating process for each material obtained through traditional (RF) and innovative methodology (PG) were recorded on a Perking Elmer FTIR spectrophotometer by UATR two infrared spectrophotometer, with a resolution of 4 cm^{-1}. The range of wavenumbers used in the analysis was from 500 to 4000 cm^{-1}. All the measurements were obtained from the solid samples at room temperature.

3.5 CWPO of paracetamol

CWPO runs were conducted in a two-necked round bottom flask of 250 mL considering 100 mL of paracetamol solution with a concentration of 100 ppm (parts per million) and pH 3.5 adjusted by the addition of H_2SO_4 solution (0.5 M). Then, the resulting solution was taken to an oil bath and coupled to a condenser and a magnetic stirring plate, which corresponds to the reaction system, represented in Figure 11. The

mixture was kept in agitation with a magnetic stirrer for 5 min to ensure thermal stability at 80 °C, which corresponds to the temperature used in the oxidation tests for paracetamol removal. After thermal stability, the stoichiometric quantity of H_2O_2 was added and then 0.25 g of catalyst was loaded into the system. The time of addition of the catalyst represents the initial moment of the reaction ($t_0 = 0$ min).

The stoichiometric amount of H_2O_2 needed for the complete mineralisation of paracetamol was calculated from Equation (11). For the degradation of a solution of paracetamol with concentration of 100 ppm, the necessary amount of H_2O_2 was determined to be 79 µL of H_2O_2 (60 %, Fisher Chemical) solution.

$$C_8H_9NO_2 + 21\,H_2O_2 \rightarrow 8\,CO_2 + HNO_3 + 25\,H_2O \quad (11)$$

During the reaction, 3 samples of 1 mL were withdrawn from the system at the intervals of 0, 5, 15, 30, 60, 120, 240, 360, 480 and 1440 min. The samples were stored in Eppendorf in the presence of Na_2SO_3 to stop the decomposition of H_2O_2 for further analysis of H_2O_2 concentration, aromaticity and paracetamol concentration. After the reaction, the catalyst was recovered by filtration, washed with distilled water and dried in air oven at 60 °C for 24 h.

Figure 11 - System used for the removal of paracetamol by CWPO.

3.5.1 Adsorption

Adsorption experiments were conducted to compare the removal efficiencies of PCM by adsorption and CWPO. In 3 Erlenmeyer flasks of 250 mL were added 25 mL of a PCM solution with a concentration of 100 ppm and pH 3.5. These Erlenmeyer flasks were inserted into an OVAN bath (Ovantherm Multiix BHM93) at a temperature of 80 °C. After thermal stabilization, 0.0625 g of sample of each catalyst studied in this work were added into the system.

After adding the materials to the system, 0.5 mL samples were withdrawn from each Erlenmeyer flask at the intervals of 0, 1, 5, 10, 30, 60, 120, 240 and 360 minutes. These samples were then diluted using a dilution factor (DF) of 16,7 since the calibration curve used to analyse the paracetamol concentration shows good sensitivity for diluted solutions. After dilution, the solutions were filtered and then the paracetamol concentration was determined by the methodology described in section 3.6.1.

3.5.2 Catalytic decomposition of H_2O_2

To study the influence of the catalyst in the process of decomposition of H_2O_2, experiments were carried out in the absence of paracetamol. Into an Erlenmeyer flask of 250 mL were added 0.125 g of catalyst, 50 mL of ultra-pure water and the corresponding stoichiometric amount of H_2O_2 (60 %, Fisher Chemical), 79 μL. The experiments were carried out at 80 °C in a OVAN Bath (Ovantherm Multiix BHM93), and the samples were withdrawn at the intervals of 0, 15, 30, 60, 120, 240, 360 and 440 min.

3.6 Analytical techniques

During the CWPO experiments, samples were regularly withdrawn from the reaction medium, filtered, and stored. Thus, H_2O_2 concentration and aromatic compound values were measured from the samples withdrawn from the system [6].

3.6.1 UV-VIS spectrophotometry

Concentration of paracetamol

The calibration curve was obtained by preparing a standard solution with a paracetamol concentration of 10 mg/L in a 20 mL volumetric flask. From this solution, 4 dilutions were made so that at the end, solutions with concentrations of 2, 4, 6, and 8 mg/L were obtained. Subsequently, each sample was analysed by UV-VIS

spectrophotometry (Jasco V-530) at the wavelength of 246 nm. The calibration curve obtained is represented in Figure 12.

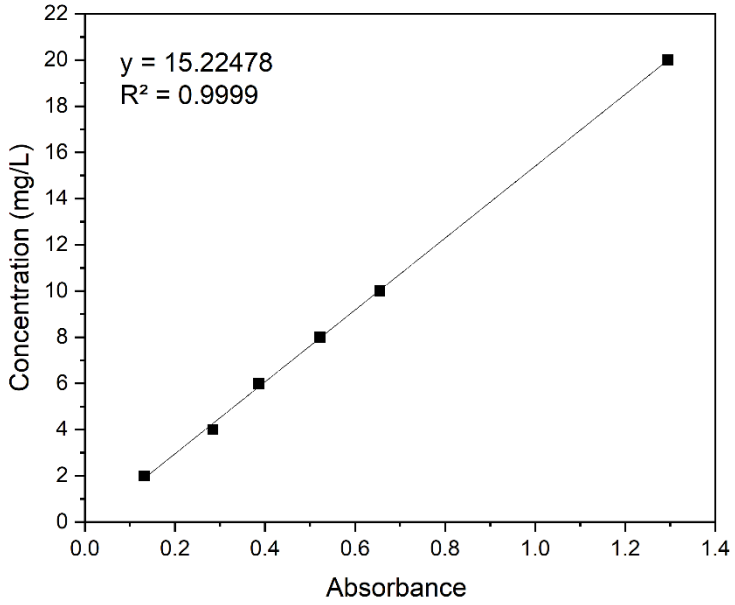

Figure 12 - Calibration curve of paracetamol at a wavelength of 246 nm. The line connecting the dots represents linear regression

Concentration of H_2O_2

To perform the determination of H_2O_2 concentration, a calibration curve was obtained based on previous work developed by the group [68] with a concentration range from 0 to 500 ppm, represented in Figure 13. To obtain the curve were added in a volumetric flask of 5 mL, 1 mL of H_2SO_4 solution (0.5 M), 0.1 mL of $TiOSO_4$ and 1 mL of solutions of H_2O_2 with different concentration, and then diluted in distilled water. Subsequently, each sample was analysed by UV-VIS spectrophotometry (Jasco V-530) at the wavelength of 405 nm. The concentration of H_2O_2 was determined by measurement of the absorbance of the yellow complex formed with tytanil sulfate ($TiOSO_4$), according to the reaction represented by Equation (12) [69].

$$TiOSO_4 + H_2O_2 + H_2SO_4 \rightarrow H_2(Ti(O_2)(SO_4)_2) + H_2O \quad (12)$$

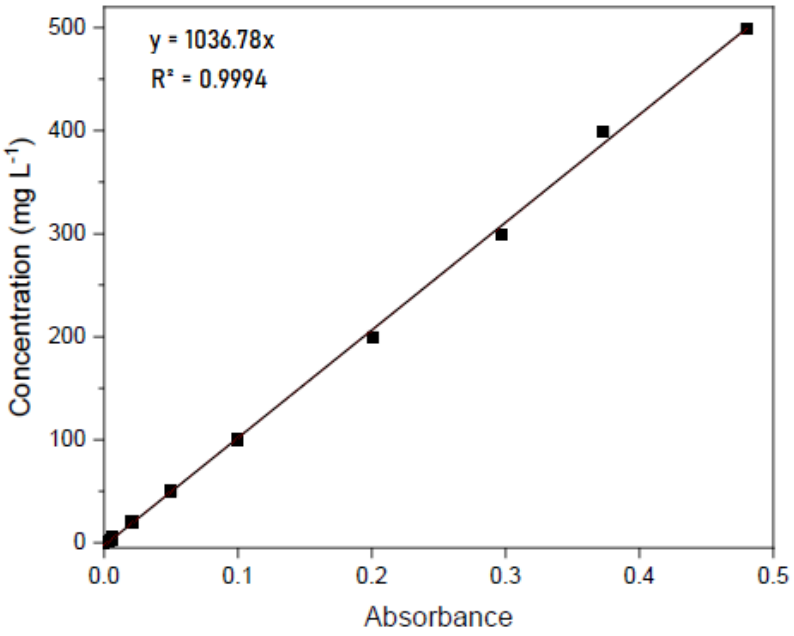

Figure 13 - Calibration curve of H_2O_2 at a wavelength of 405 nm. The line connecting the dots represents linear regression

The linear regression showed an R^2 of 0.9994, revealing the good quality of the calibration curve built. This result allows the quantification of H_2O_2 concentration from the absorbance of the samples.

Aromatic compounds

The analysis for quantification of aromatic compounds formed is described elsewhere [70]. To ensure that the pH of the reaction medium does not interfere in the analysis of the aromatic compounds, a phosphate buffer solution (PBS) of H_3PO_4 with pH 7.0 was prepared. Subsequently, 0.5 mL of the samples were diluted in a volumetric flask of 5 mL using PBS as solvent. Thereafter, the sample was analysed by UV-VIS spectrophotometry (Jasco V-530) at the wavelength of 254 nm.

PCM also absorbs at the wavelength of 254 nm. Thus, in the samples obtained during the analysis, it is necessary to subtract the absorbance of paracetamol from the total absorbance of the samples obtained during the analysis, in order to obtain the real absorbance of the aromatic compounds present in the reaction medium.

From the concentration of PCM obtained by HPLC analysis it is possible to determine the relative absorbance of paracetamol in each of the analysis samples by means of the calibration curve represented by Figure 14.

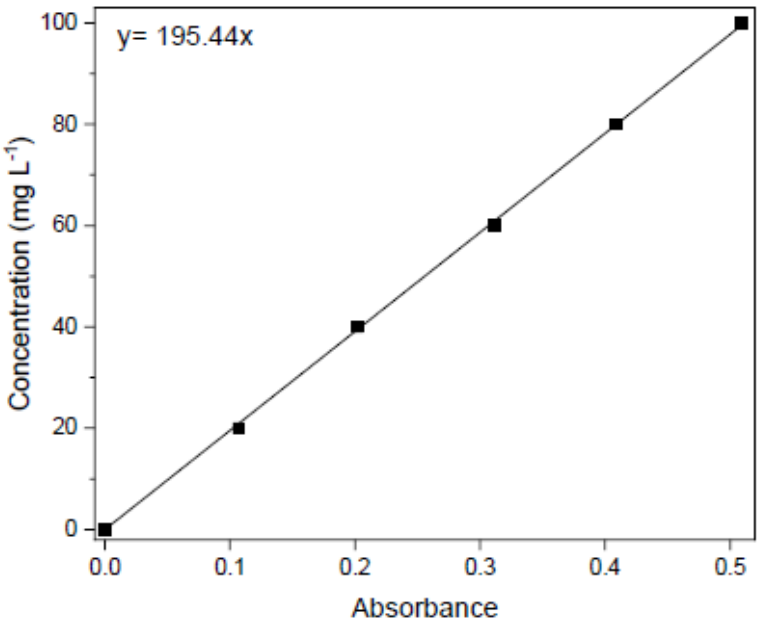

Figure 14 - Calibration curve of paracetamol for aromaticity analysis. The line connecting the dots represents linear regression

To determine the quantity of aromatic compounds, the value obtained for the relative absorbance of paracetamol is subtracted from the total absorbance obtained. The amount of aromatic compounds expressed in percentage for each of the reaction collection times can be obtained by means of Equation (13):

$$Aromatics\ (\%)_t = \frac{ABS_{Total,t} - ABS_{PCM,t}}{ABS_{PCM,0}} \quad (13)$$

Where ABS_{Total} represents the total absorbance analysed and ABS_{PCM} represents the relative absorbance of paracetamol at different times of reaction.

Iron concentration

The amount of iron in the samples after CWPO was determined by atomic absorption, using the equipment SpectrAA Varian equipped with a Varian hollow cathode lamp in a wavelength of 248.3 nm. Figure 15 represents the calibration curve obtained in a concentration range of 0.1-5.0 mg/L.

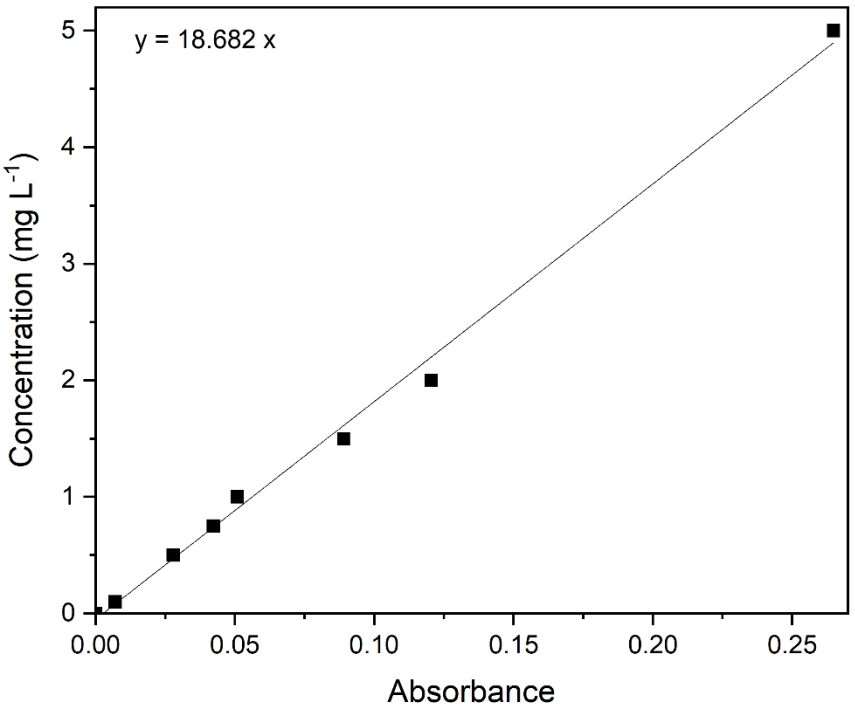

Figure 15 - Calibration curve of iron concentration.
The line connecting the dots represents linear regression

3.6.2 High Pressure Liquid Chromatography (HPLC)

To determine the concentration of paracetamol and possible intermediate compounds formed during the CWPO runs, was used a High-Pressure Liquid Chromatograph (HPLC) Jasco equipped with a UV-VIS detector (UV-2075 Plus), a quaternary gradient pump (PU-2089 Plus) for solvent delivery, and an Ultra Biphenyl Column (L11) 100 Å (150 mm x 2.1 mm) RESTEK. For this analysis, 20 µL aliquots were injected manually into the chromatograph by a current flow of 0.300 mL/min consisting of a mixture of phosphate-buffer/acetonitrile (95:5 v/v) fed for 6 min, followed by a gradient elution to reach (65:35 v/v) of phosphate-buffer/acetonitrile from 6 min to 12 min, maintaining this proportion until 18 min and, subsequently, gradient elution from 18 min to 30 min until reaching the initial mobile phase ratio (95:5 v/v). The wavelength used for peaked absorbance detection of Paracetamol, Hydroquinone, *p*-Benzoquinone, and 4-Nitrophenol was 246 nm.

It is well known that in CWPO process of paracetamol degradation can lead to a formation of intermediate organic compounds, due to the non-selective degradation caused by $HO^{\bullet}$ radicals [5]. To evaluate and identify the possible intermediates that was maybe formed during CWPO reaction for paracetamol degradation, substances

such as hydroquinone, *p*-benzoquinone, 4-nitrophenol, resorcinol, phloroglucinol, catechol, phenol and pyrogallol were injected into HPLC to analyse the residence time for each of them. The choice of those substances was based on the paracetamol pathway reported in literature [32,68,69].

3.7 Catalyst reusability

After the oxidation tests, the catalyst was recovered from the reaction medium by applying an external magnetic force (magnet). Thereafter, the catalyst was washed several times with distilled water and the solvent were subsequently changed from water to ethanol. The solid material was then dried in an oven under a temperature of 60 °C for 16 h. After dried, the catalyst was used in a new oxidation cycle under the same operation conditions.

RESULTS AND DISCUSSIONS

4 RESULTS AND DISCUSSION

4.1 Characterization of materials

The materials prepared as catalysts in the present work were analysed via Fourier Transform Infra-Red (FT-IR) and adsorption isotherms of N_2 at 77 K.

4.1.1 FT-IR analysis

The FT-IR spectra of the materials resultant of the three steps of carbon-coating were obtained in order to identify functional groups and chemical structural changes. The results obtained are represented in Figure 16. It is possible to see that, due to the energy of radiation, each composition attained some vibrational bands at certain wavenumbers.

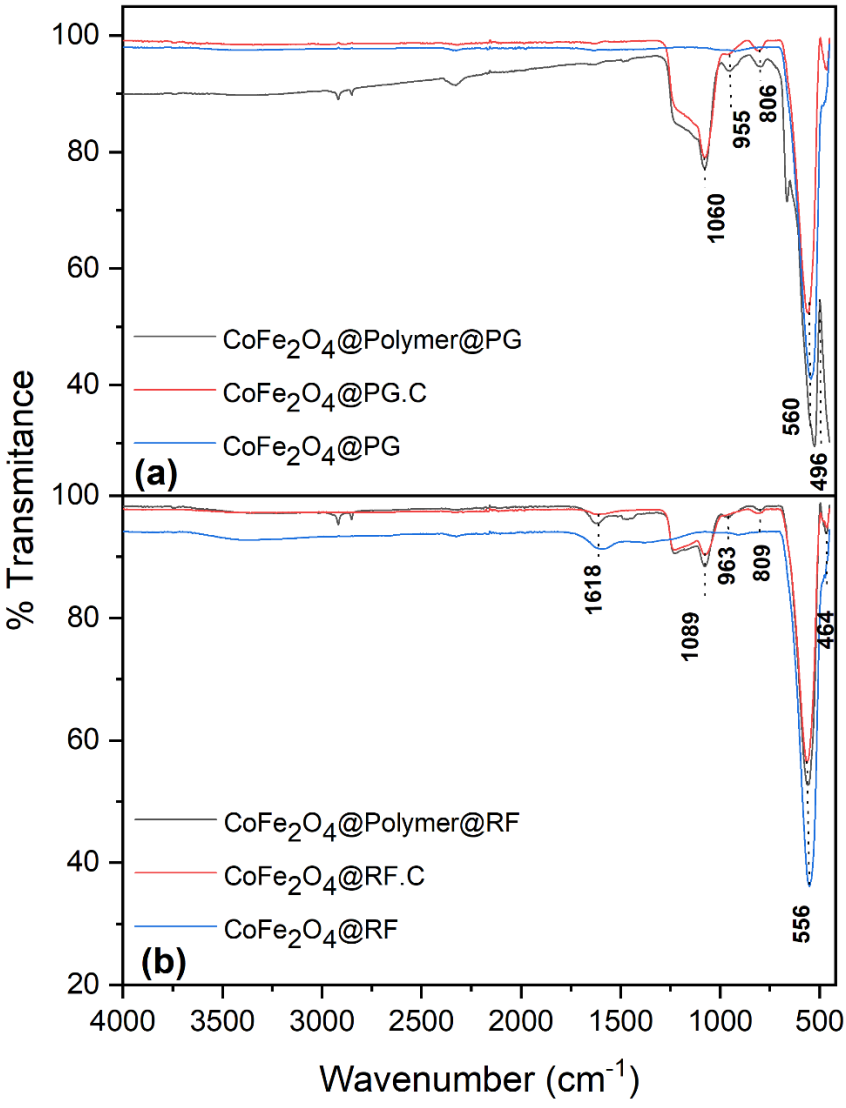

Figure 16 - FTIR spectra of (a) materials prepared using phloroglucinol and glyoxalic acid or (b) resorcinol and formaldehyde.

Two main peaks were observed at 496 and 560 cm^{-1} in Figure 16 (a), for the 3 materials prepared with phloroglucinol and glyoxalic acid, and at 464 and 556 cm^{-1} in Figure 16 (b), for the three materials prepared with resorcinol and formaldehyde. The peaks between 460 and 500 cm^{-1} are attributed to the stretching vibration of octahedral sites, indicating the Co-O bond, while the peaks observed at a wavenumber around 560 cm^{-1} are attributed to the tetrahedral sites of Fe-O bond, these results suggest the chemical bonds between the cobalt oxides and the iron oxide, indicating a possible formation of the cobalt ferrite structure [71]. A strong and wide absorption band around 1060 and 1089 cm^{-1} were also observed for $CoFe_2O_4$@Polymer@RF, $CoFe_2O_4$@Polymer@PG, $CoFe_2O_4$@PG.C and $CoFe_2O_4$@RF.C, which are attributable to Si-O-Si stretching vibrations, while the absorption bands around 800 and 960 cm^{-1} are assigned to Si-O symmetric stretching vibrations [72].

Moreover, the peak observed at 1618 cm^{-1} for the materials prepared by the traditional methodology (RF) is attributed to the bending vibration of H-O-H molecules and associated to the presence of water. For the final materials ($CoFe_2O_4$@PG and $CoFe_2O_4$@RF, obtained through innovative and traditional methodology), no signal related to Si-O-Si bonds were observed. Hence, FT-IR analysis results suggest the completely removal of SiO_2 by NaOH (10 mol L^{-1}) after etching process [72,73].

4.1.2 Textural properties

Nitrogen sorption isotherms of the carbon-based magnetic nanoparticles obtained through carbonization of Resorcinol-Formaldehyde and Phloroglucinol-Glyoxylic acid polymeric resins are shown in Figure 17. It can be seen that all materials show typical type IV isotherms with type H2 hysteresis, according to the classification established by IUPAC [67]. This type of isotherm is given by mesoporous materials in which the adsorption behaviour is determined by the adsorbent-adsorptive interactions and the interactions between the molecules in the condensed state. Moreover, H2 hysteresis loops have been observed for mesoporous ordered silicas after thermal treatment [67,74]

The surface areas of the materials were also evaluated via BET method after thermal treatment under N_2 inert atmosphere and after washing with NaOH to remove the silica formed during the polymerization of TEOS. The results of surface area as well as the total pore volume are presented in Table 2.

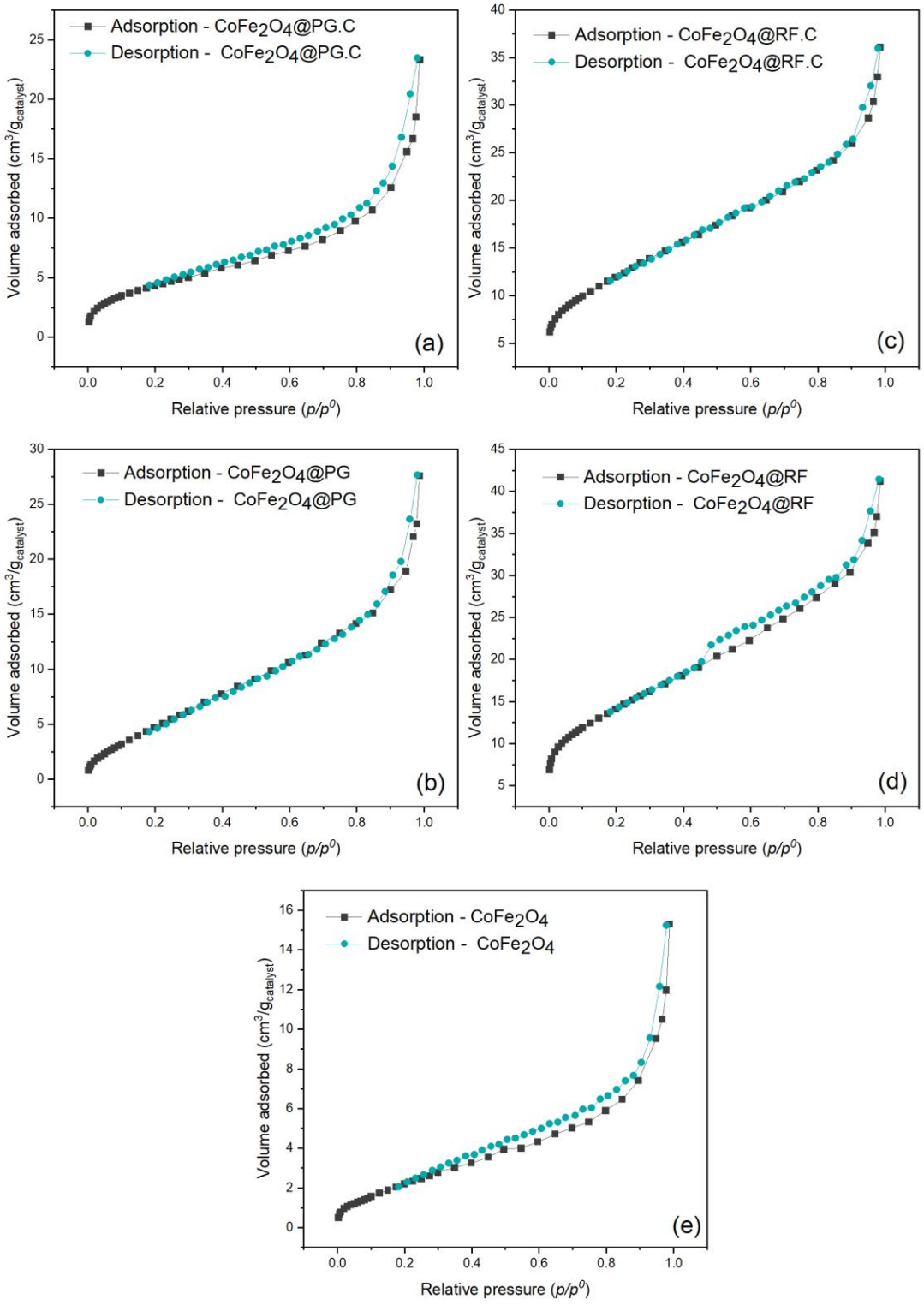

Figure 17 - N_2 adsorption and desorption isotherms at 77 K of the nanomaterials prepared in different steps: (a-b) after annealing; (c-d) after etching with NaOH; (e) core.

Table 2 - Textural properties of produced materials

Material	S_{BET} $(m^2 g^{-1})$	Total pore volume $(mm^3 g^{-1})$
$CoFe_2O_4$	9	0.0196
$CoFe_2O_4$@PG.C	16	0.0320
$CoFe_2O_4$@PG	22	0.0380
$CoFe_2O_4$@RF.C	43	0.0530
$CoFe_2O_4$@RF	57	0.0600

The coating of the core by a carbon layer by means of the use of two methodologies proposed in the work (PG and RF) lead to an increase in the surface area of the material when compared to its bulk state, as $CoFe_2O_4$ (bare core). The results obtained are in agreement with those reported in the literature [33,35,72,75], since the coating of the catalyst core has as one of its main functions the increase of the surface area, leading to an increase in the number of active sites available for catalytic reactions.

4.2 Development of HPLC method for monitoring oxidized intermediates of paracetamol

The degradation of paracetamol is a complex reaction mechanism, with several smaller molecules being obtained from the initial molecule. The sort of intermediate compounds formed is related to the breaking down of the bond between the functional groups that compose its structure [76]. Several studies [77,78] have reported the different organic substances that can be formed during the pathway of paracetamol degradation, Figure 18.

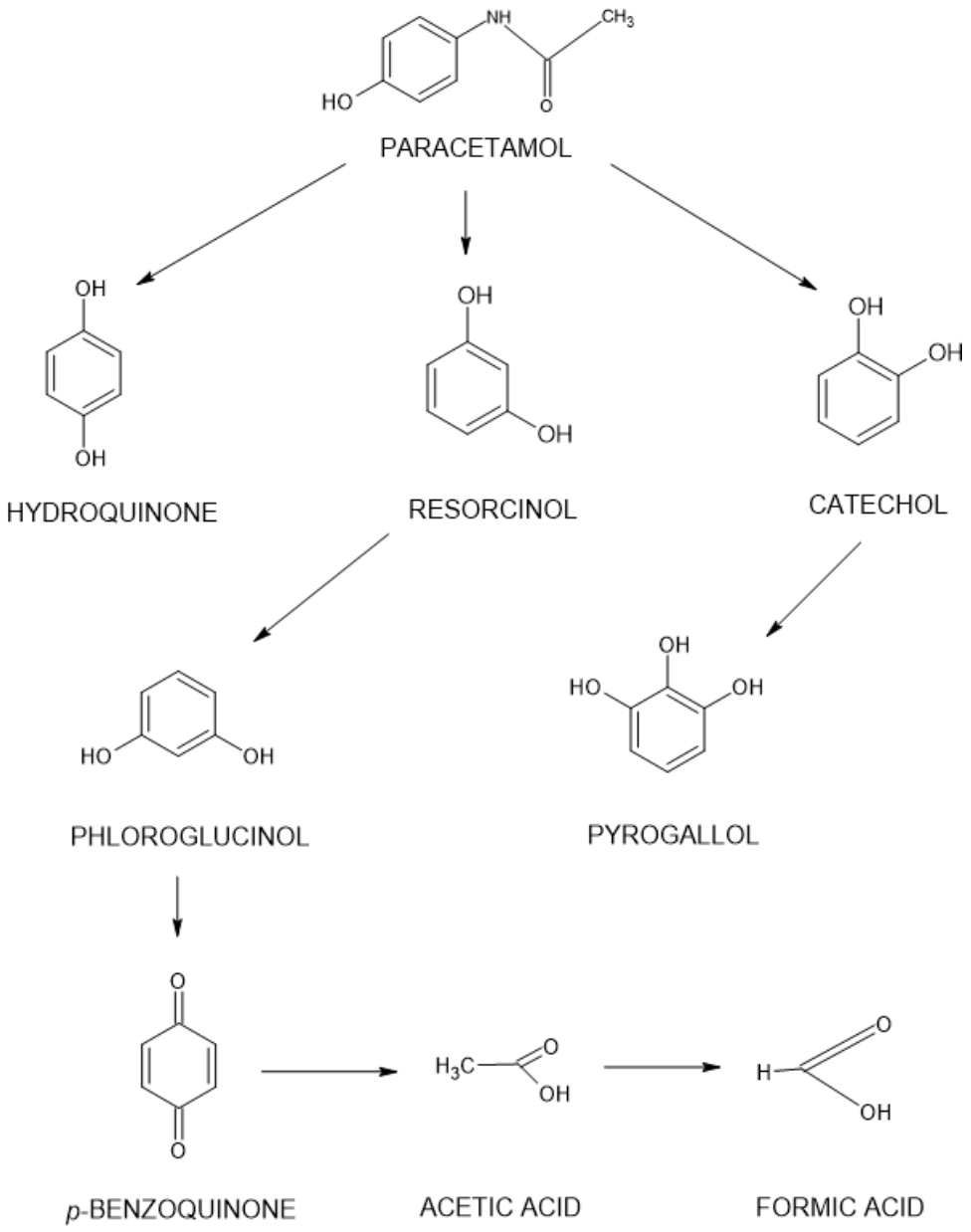

Figure 18 - Oxidation pathway proposed for degradation of paracetamol. Adapted from [76].

A previous study was performed with the injection of hydroquinone, *p*-benzoquinone, paracetamol and 4-nitrophenol solutions in HPLC at different absorption wavelengths (210, 246, 277, and 318 nm), to evaluate at which wavelength the highest values of area under curve were obtained for both paracetamol and some of the intermediate compounds that can be formed during its degradation. The choice of wavelengths was based on the literature [79], which it was reported that the best sensitivities for hydroquinone, *p*-benzoquinone, 4-nitrophenol and paracetamol were obtained at the respective wavelengths of 371, 246, 318 and 246 nm.

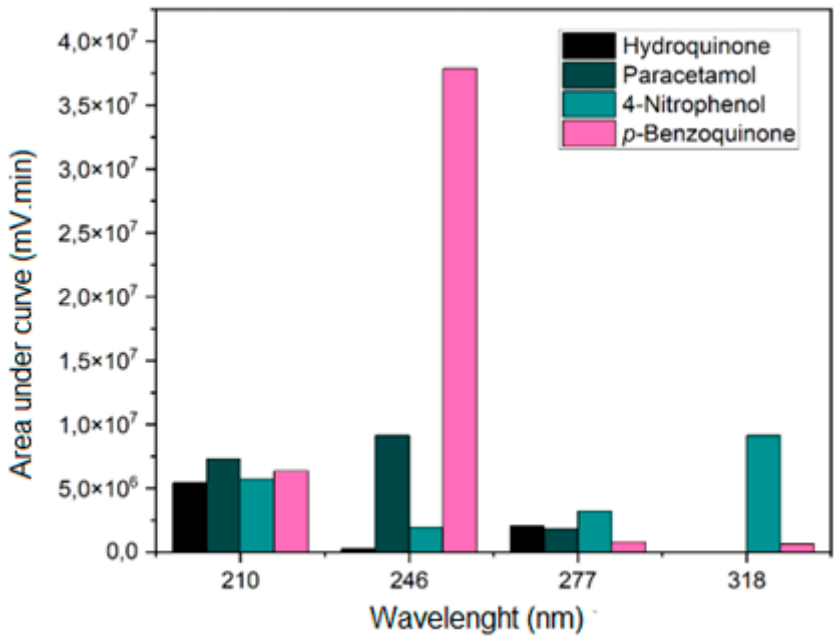

Figure 19 - Response of compounds at different wavelengths for the same concentration (25 mg L^{-1}).

By observation of Figure 19, it was possible to conclude that the highest values of area under the curve were obtained for paracetamol and for *p*-benzoquinone at a wavelength of 246 nm. In addition, at the wavelength of 246 nm it was also possible to verify a good sensitivity for 4-nitrophenol and *p*-benzoquinone. Therefore, the model pollutant and its oxidized intermediates can be properly monitored in CWPO process by HPLC at 246 nm, using the stationary and mobile phase described in the methodology.

Table 3 shows the average retention time as well the area under curve observed for some possible intermediate compounds from paracetamol degradation. All the retention times for the compounds were analysed by HPLC under the same methodology described in the section 3.6.2. Thus, by comparing the retention time of the intermediate compound formed during CWPO and the retention times shown in Table 3, it is possible its identification.

Table 3 - Retention times for different compounds at same concentrantion of 25 mg L^{-1} obtained by HPLC using the stationary and mobile phase described in the section 3.6.2.

Compound	Average retention time (min)	Area under curve
Phloroglucinol	3.050	3798322
Hydroquinone	3.583	4098637
Pyrogallol	3.605	7261300
Resorcinol	4.960	3268036
p-Benzoquinone	5.682	26193175
Catechol	6.458	3311496
Phenol	12.19	1435565
4-Nitrophenol	16.80	3513721

4.3 CWPO of paracetamol

The results of CWPO of PCM, as well as H_2O_2 decomposition obtained with each catalyst are represented in Figure 20 (a) and Figure 20 (b). The representation of the relative concentration profiles was shown in groups taking in to account the synthesized materials $CoFe_2O_4$, $CoFe_2O_4$@RF, $CoFe_2O_4$@PG, and non-catalyst.

From the results showed in Figure 20 (a) and (b), it is observed that without catalyst the decomposition of H_2O_2 and the removal of PCM are not significant, since only 10 % of H_2O_2 decomposition and 13 % of pollutant removal were obtained after 24 h of reaction time. The decomposition of hydrogen peroxide observed in the non-catalytic reaction is related to thermal decomposition, and this amount of decomposed H_2O_2 was enough to promote the degradation of 13% of the initial concentration of the pollutant in the system.

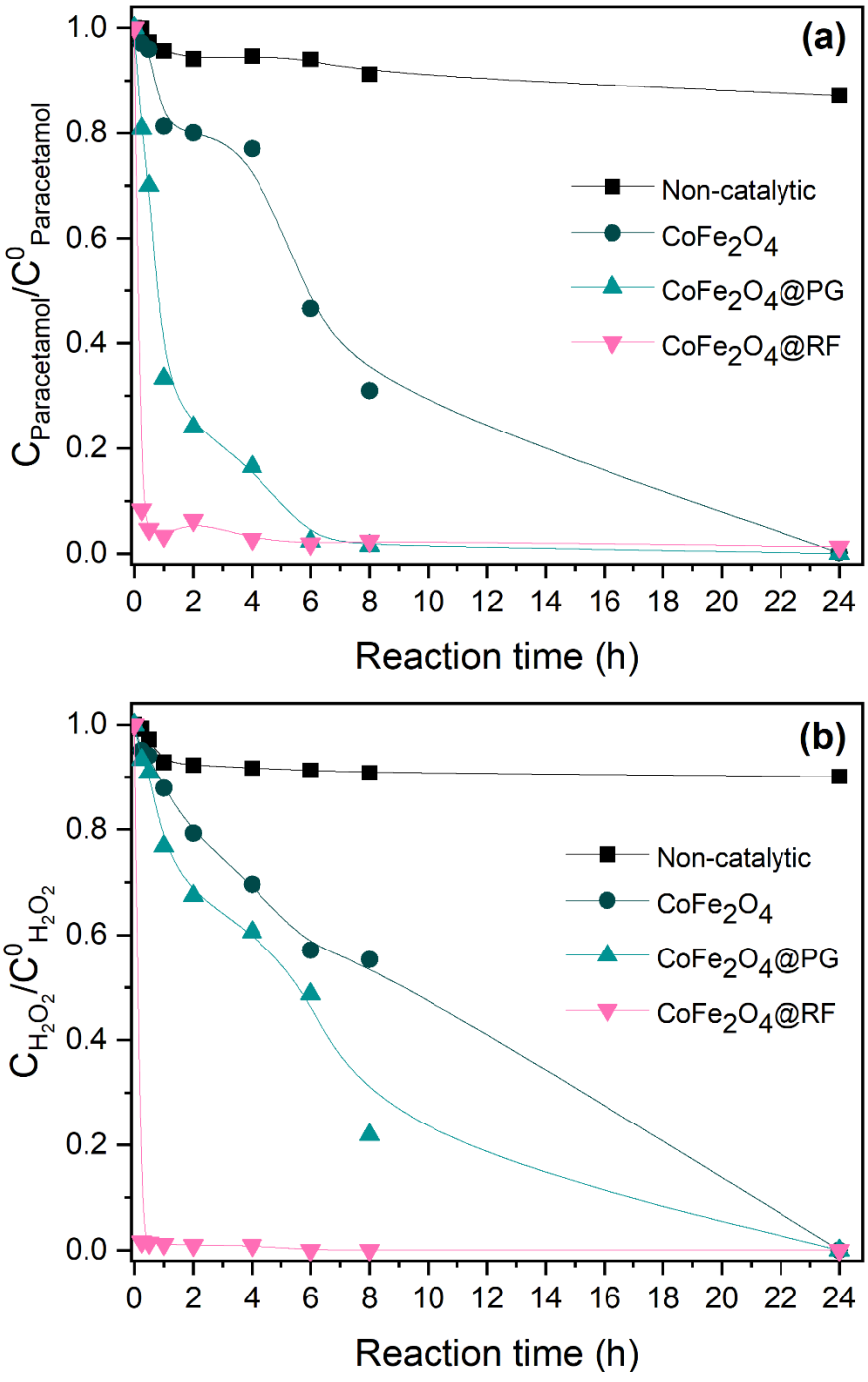

Figure 20 - Normalized concentration of (a) PCM in CWPO, (b) H_2O_2 in CWPO throughout reaction. Operational conditions: $C_{PCM,0}$ = 100 mg·L^{-1}, $C_{H2O2,0}$ = 472.4 mg·L^{-1}, C_{cat} = 2.5 g·L^{-1}, pH_0= 3.5 and T = 80 °C. (lines connecting points are only indicating trends)

Regarding decomposition of H_2O_2, as can be observed in Figure 20 (b), the slowest degradation was obtained in the oxidation run conducted for $CoFe_2O_4$, which has showed a decomposition of H_2O_2 of 43% after 6 hours. On the other hand, different profiles of decomposition were observed for the reactions carried out with the carbon-

coated materials, $CoFe_2O_4$@PG and $CoFe_2O_4$@RF, revealing values of H_2O_2 decomposition of 52% and 100% after 6 hours, for the receptive catalysts, indicating a high activity for the decomposition of hydrogen peroxide. Moreover, the material $CoFe_2O_4$@RF has shown a faster decomposition amongst the other materials tested, which a total degradation of H_2O_2 was observed after 15 minutes of reaction time. The higher activity of $CoFe_2O_4$@RF can be ascribed to its high surface area, resulting in a larger amount of electron donating actives sites available for H_2O_2 decomposition [25,39]. Thus, the order of reactivity of the materials in hydrogen peroxide decomposition can be described as $CoFe_2O_4$@RF > $CoFe_2O_4$@PG > $CoFe_2O_4$.

The order in the reactivity of catalysts for the oxidation of paracetamol was the same as that observed for the decomposition of H_2O_2, Figure 20 (b). For the most reactive sample, $CoFe_2O_4$@RF, which produced the highest decomposition of H_2O_2 in a short period of time, a very fast decomposition of paracetamol was reached at the beginning of CWPO, leading to a complete removal of the pollutant after 1 h of reaction. For the catalysts that showed a slower hydrogen peroxide decomposition profile, the kinetics of pollutant removal also occurred more slowly. The results presented in Figure 20 (a) show that after 6 h of reaction time, the catalyst $CoFe_2O_4$@PG was able to promote a fully removal of paracetamol from the system with a decomposition of H_2O_2 of 52%, while for the same period, the uncoated catalyst $CoFe_2O_4$ reached 57% of paracetamol removal and 43% of H_2O_2 decomposition.

From the results obtained it is possible to observe that all catalysts were able to promote the total decomposition of H_2O_2 and the full removal of paracetamol after 24 h of reaction time. In addition, is also possible to observe that the carbon-coated magnetic nanoparticles have improved the results of decomposition and pollutant removal when compared to the uncoated material, $CoFe_2O_4$.

The combination of active iron species with carbon-based nanomaterials promotes a synergistic effect that increase the performance of the carbon materials in CWPO. This can be explained by the electron donor characteristics of both metals that compose the structure of the material and the carbon layer that coats the core of the catalyst. Electron transfer is the necessary condition to promote the degradation of H_2O_2 leading to the formation of hydroxyl radicals and, consequently, to the removal of the pollutant from the system [39].

Velichkova et al [80] have reported the oxidation of paracetamol using iron oxide magnetic nanoparticles in a heterogenous-Fenton process. The reaction was performed with the same initial concentration of pollutant, stoichiometric amount of hydrogen peroxide and catalyst dosage of 6 $g \cdot L^{-1}$ leading to the fully removal of paracetamol after 5 h of reaction time. However, the quantity of catalyst dosage was more than twice of the catalyst dosage used in this present work, in which after 6 h the fully degradation of paracetamol was obtained with both catalysts $CoFe_2O_4$@PG and $CoFe_2O_4$@RF.

At the end of the treatment via CWPO the final effluents of reactions were analysed in order to study the contribution that the coating provides to the catalyst core in terms of protection of the active phase against the iron leaching. The results obtained are expressed in Table 4.

Table 4 - Iron leached at the end of CWPO process

Materials	Concentration of leached iron (mg/L)	Leaching of Iron (wt%)
$CoFe_2O_4$ – Core	2.6823	2.2538
$CoFe_2O_4$@RF	0.9020	0.7578
$CoFe_2O_4$@PG	0.4535	0.3811
Non-catalytic	0.0001	N. A.

*N. A. = Not Applied

As observed through the data expressed in Table 4, the reaction conducted by the material $CoFe_2O_4$ has shown the highest concentration of leached iron at the end of the CWPO process. This value is higher than that established by the law of Portugal and other EU countries, which determines that the maximum concentration of iron present in treated water and discharged into natural bodies of water should not exceed the concentration 2 $mg \cdot L^{-1}$ [58].

For the reactions conducted by the catalysts $CoFe_2O_4$@RF and $CoFe_2O_4$@PG the respective concentration values of 0.90 and 0.45 $mg \cdot L^{-1}$ were observed. Both materials obtained by coating the core via traditional (RF) and alternative (PG) coating promoted greater stability and protection of the active phase, leading to lower concentrations of leached iron at the end of the treatment process. The most stable material among the

materials studied is $CoFe_2O_4$@PG, since it presented the lowest concentration of leached iron.

To differentiate whether the pollutant is just being adsorbed on the catalyst surface or is being removed via oxidation, a preliminary study in the absence of hydrogen peroxide was carried out.

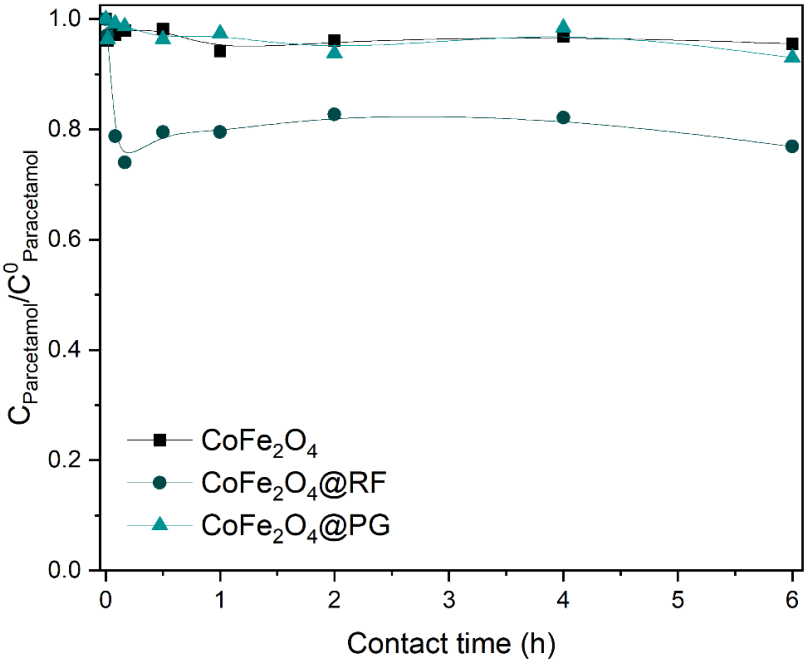

Figure 21 - Normalized concentration of PCM in adsorption runs without H_2O_2. Operational conditions: $C_{PCM,0}$ = 100 mg·L^{-1}, C_{cat} = 2.5 g·L^{-1}, pH_0= 3.5 and T = 80 °C. (lines connecting points are only indicating trends).

As observed in Figure 21 the removal of the pollutant by adsorption were 4.5, 23.2, and 7.1% after 6 h of contact time for the respective catalysts, $CoFe_2O_4$, $CoFe_2O_4$@RF and $CoFe_2O_4$@PG. These results reveal the higher interaction of the pollutant and the $CoFe_2O_4$@RF carbon-coated nanomaterial when compared to the uncoated catalyst, this catalyst presented a larger specific area and consequently a larger amount of active sites available for adsorption of the pollutant on the catalyst surface. However, according to the results it is possible to verify that the adsorption process is not sufficient to perform the complete removal of paracetamol from the system, since after 6 h of contact more than 70 % of the initial pollutant amount is still present in the system, for all the catalysts studied.

4.4 Decomposition of hydrogen peroxide

Several processes can explain the observed increase of catalytic activity of the carbon coated materials in the oxidation of paracetamol by CWPO. Amongst them it is possible to highlight the competitive adsorption of pollutants and hydrogen peroxide at the catalyst surface, the decomposition of hydrogen peroxide molecules at the catalyst surface to produce reactive hydroxyl radicals, the reaction of the generated hydroxyl radicals with either the pollutant molecules or with other hydrogen peroxide molecules, the adsorption of pollutant molecules nearby the active sites that generates HO• radicals, among other process.

To evaluate the competition between hydrogen peroxide and paracetamol molecules, an experiment of H_2O_2 decomposition was performed in the absence of paracetamol, under same operation conditions described previously. The results obtained are presented in Figure 22.

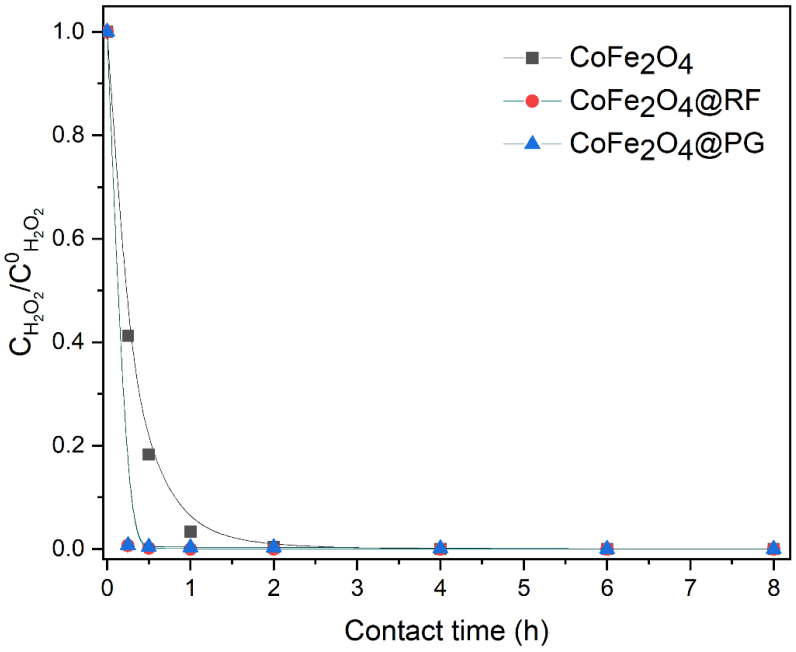

Figure 22 - Normalized concentration of H2O2 throughout reaction.
Operational conditions: $C_{H2O2,0}$ = 472.4 mg·L^{-1}, C_{cat} = 2.5 g·L^{-1}, pH_0 = 3.5 and T = 80 °C.
(Lines connecting points are only indicating trends).

Both $CoFe_2O_4$@PG and $CoFe_2O_4$@RF catalysts promoted the total decomposition of H_2O_2 in 15 minutes of reaction, while with the $CoFe_2O_4$ catalyst the total degradation was obtained only after 1 h of reaction. Comparing the H_2O_2 decomposition profiles shown in Figure 22 with the decomposition profiles shown in

Figure 20 (b), it can be seen that the decomposition of H_2O_2 in the reaction conducted by $CoFe_2O_4$@PG was slower in the presence of PCM, reaching only 24% of H_2O_2 decomposition after 1 h of reaction time. This result indicates that PCM competes with H_2O_2 for the active sites available on the catalyst surface, leading to a more selective and efficient H_2O_2 decomposition, as the hydroxyl radicals produced interact with the PCM molecules adsorbed in the vicinity of the active sites [81].

4.5 Oxidized intermediates and aromatics compounds

Figure 23 shows the formation and further oxidation of aromatic compounds produced during CWPO. The concentration of aromatic compounds was evaluated during 24 h of paracetamol oxidation.

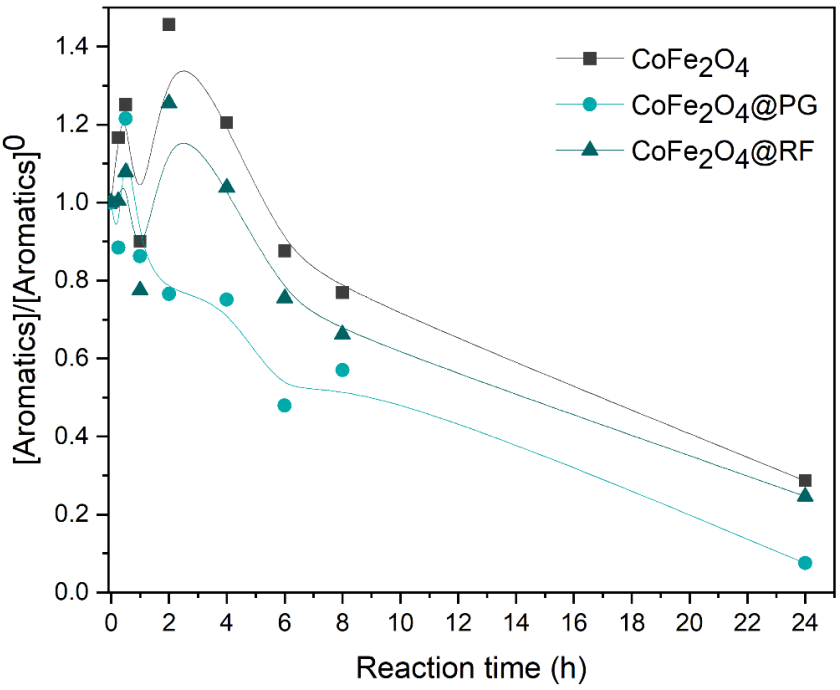

Figure 23 - Normalized concentration of aromatic compounds. Operational conditions: $C_{PCM,0}$ = 100 mg·L^{-1}, $C_{H2O2,0}$ = 472.4 mg·L^{-1}, C_{cat} = 2.5 g·L^{-1}, pH_0 = 3.5 and T = 80 °C. (Lines connecting points are only indicating trends).

For the reactions performed with $CoFe_2O_4$ and $CoFe_2O_4$@RF, an increase in the initial concentration of aromatic compounds of 25 and 7% was observed for the respective catalysts within 30 min after initiation of CWPO. The increase in the concentration of aromatics in relation to the initial concentration is related to the different degradation pathways that paracetamol can undergo, leading to the formation of several intermediate compounds during its oxidation process.

In addition, the maximum concentration of aromatic compounds observed for the same catalysts occurred in the interval of 2 h after starting the reaction, in which an increase of 45% for $CoFe_2O_4$ and 25% for $CoFe_2O_4$@RF was observed. In addition, after 2 h of reaction both catalysts showed similar profiles of reduction of aromatic compounds concentration along the reaction, so that after 24 h of reaction it was observed that 28 and 24 % of the initial concentration of aromatic compounds for the respective catalysts remained in the reaction medium.

The concentration profile of the aromatic compounds obtained for the reaction conducted with $CoFeO_4$@PG showed a different behaviour from the others. As can be seen in Figure 23 the use of this catalyst led to an increase in the concentration of these compounds in the initial intervals of the reaction, so that the maximum increase in relation to the initial concentration observed was 21% after 30 minutes of reaction. After this initial increase, a concentration decrease profile higher than the other catalysts was observed, so that after 24 h of reaction only 8% of the initial concentration of aromatic compounds remained in the system. Thus, comparing the results obtained by means of reduction in the concentration of aromatic compounds over the 24 h of reaction, the activity of the catalysts can be classified as $CoFe_2O_4$@PG > $CoFe_2O_4$@RF > $CoFe_2O_4$.

The faster decrease of the initial concentration of aromatic compounds observed with $CoFe_2O_4$@PG may be associated with the degradation of the aromatic compounds produced during the paracetamol degradation pathway, since the material $CoFe_2O_4$@PG led to obtain the highest removal of PCM. Hence it is expected to show higher catalytic activity for the oxidation of the oxidized intermediates among the other materials studied in this work.

Moreover, it was observed through the reactions conducted with $CoFe_2O_4$ and $CoFe_2O_4$@PG the presence of a peak in the chromatographic analyses with a residence time of 13.4 minutes between the intervals of 15 and 360 minutes, Figure 24.

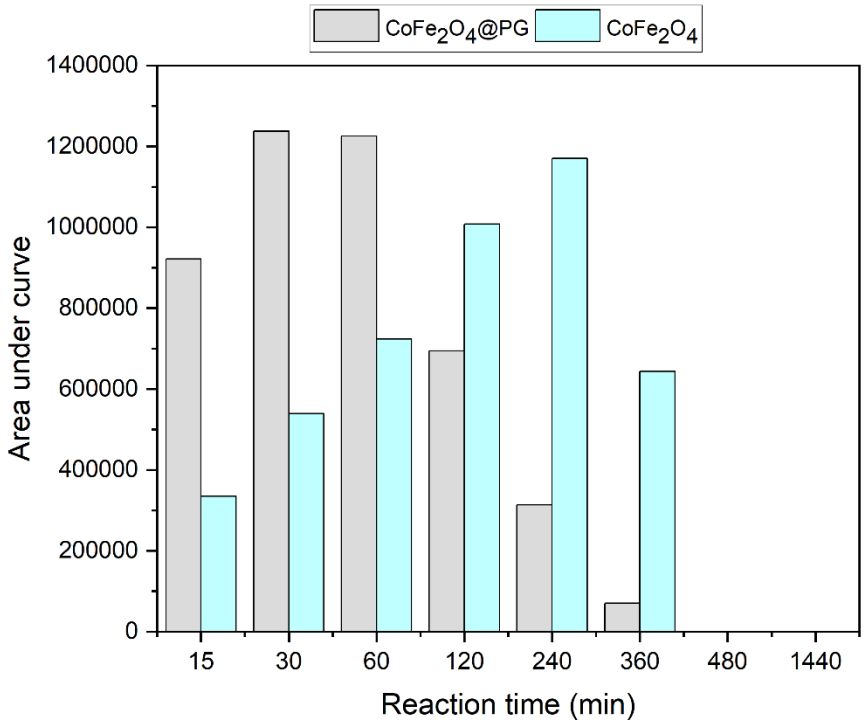

Figure 24 - Area under curve for the intermediate compound analysed by HPLC methodology

By means of Figure 24, it was possible to visualise that the largest area over the curve for this compound was for the intervals of 15 to 30 minutes for the $CoFe_2O_4$@PG catalyst and between 120 and 240 minutes for the $CoFe_2O_4$ catalyst. This result is in line with the results obtained in Figure 23, since the maximum concentration of aromatic compounds for the $CoFe_2O_4$ catalyst was obtained in the intervals between 2 and 4 h while for the $CoFe_2O_4$@PG catalyst was obtained in the initial intervals of reaction, between 30 and 60 minutes. However, the residence time observed through the chromatographic analyses for this peak is different from the residence time of the compounds that were calibrated, Table 3. Thus, this result suggests the formation of an intermediate compound formed in the initial moments of reaction and its subsequent degradation after 360 minutes of reaction.

4.6 Catalyst Reusability

An experiment to study catalyst reusability during three successive CWPO reactions was carried out with $CoFe_2O_4$@PG, which was the catalyst that showed a more selective hydrogen peroxide decomposition profile consistent with the progressive decrease in paracetamol concentration and to the greatest decrease in the concentration of aromatic compounds over the 24 h of reaction. The obtained results are presented in Figure 25.

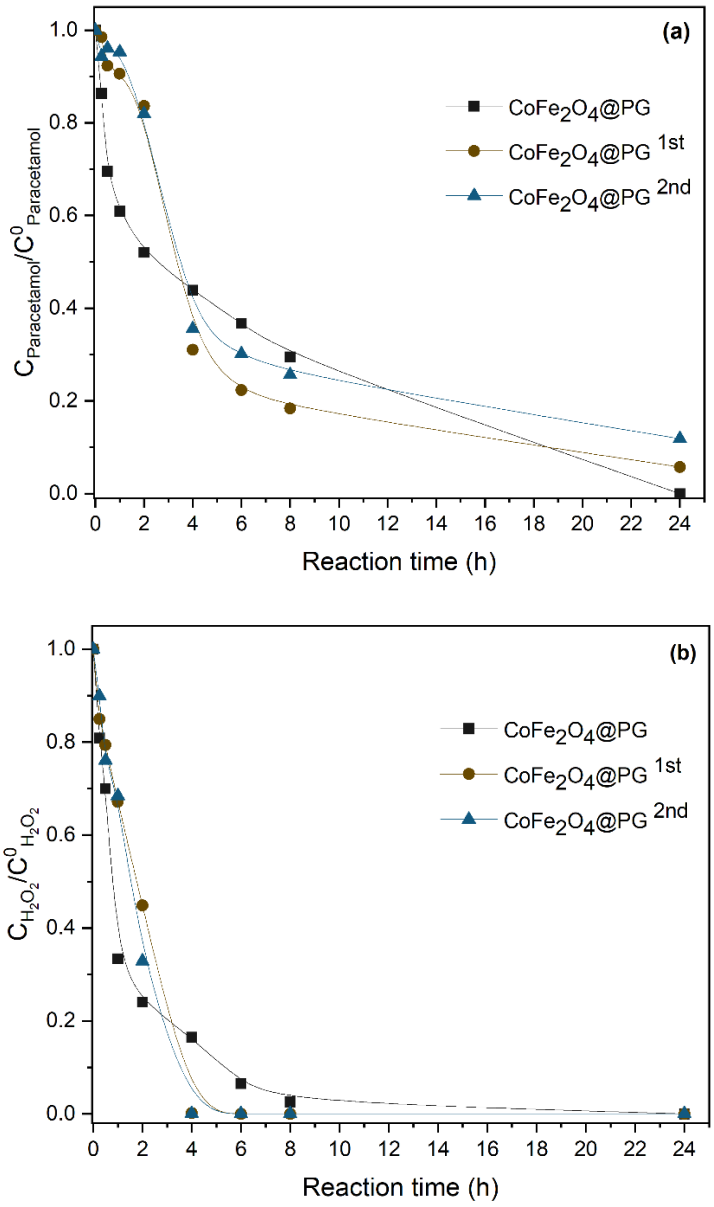

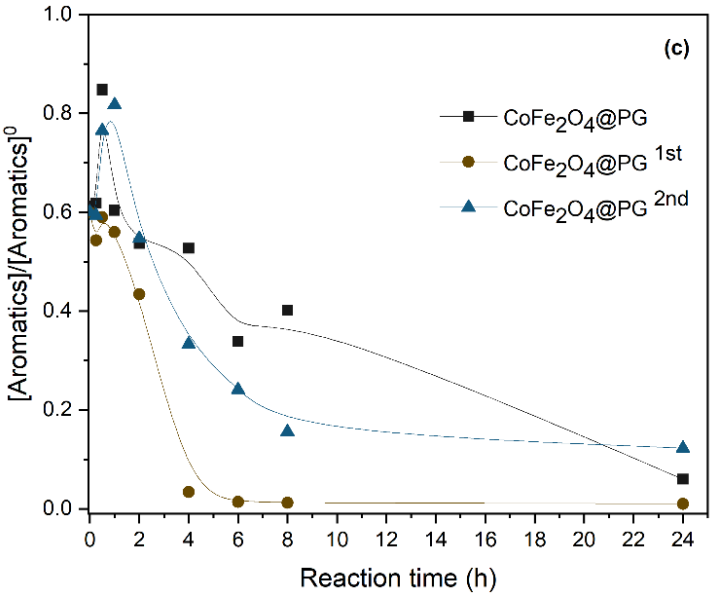

Figure 25- Normalized concentration of (a) PCM, (b) H_2O_2 and (c) aromatics along reaction time. Operational conditions: $C_{PCM,0}$ = 100 mg·L^{-1}, $C_{H2O2,0}$ = 472.4 mg·L^{-1}, C_{cat} = 2.5 g·L^{-1}, pH_0 = 3.5 and T = 80 °C. (Lines connecting points are only indicating trends)

As can be observed in Figure 25 (a) and (b), the removal profiles of paracetamol and hydrogen peroxide in the first and second reaction cycles were similar. For both oxidation reactions a complete removal of paracetamol was observed in 4 h of reaction, representing an increase of 17% in the removal efficiency when compared to the first use of the catalyst. No obvious loss of catalytic activity was observed for paracetamol degradation, and the removal efficiency was quite similar during the cycles, indicating that the material is very stable during the reaction.

The reutilization tests also show that the catalytic activity of $CoFe_2O_4$@PG slightly improved for paracetamol removal compared to the first run. This behaviour can be related to changes in the surface chemistry of the catalyst by oxidation in the first contact with hydrogen peroxide, which changes its catalytic properties.

The recovery and reuse of the catalyst with the same degradation efficiency represent one of the main advantages of the use of heterogeneous Fenton methodology, leading to a reduction of the operation cost with a lower environmental impact [82]. Thus, these characteristics make this process attractive for wastewater treatment.

The concentration of aromatic compounds throughout the reaction was also investigated, Figure 25 (c). Different profiles of decrease in the concentration of aromatic compounds for the first and second reactions were obtained. The first reaction presented the best result in relation to the other oxidation runs, in which a 100% decrease of the

initial concentration of aromatic compounds was observed after 4 h, while for the same reaction interval the respective concentration decreases are of 48 and 67% for $CoFe_2O_4$@PG and $CoFe_2O_4$@PG ^{2nd}.

The reactions conducted with $CoFe_2O_4$@PG and $CoFe_2O_4$@PG^{1st} have led to a complete removal of the aromatic compounds after 24 h of reaction. For the same reaction interval, the reaction carried out with $CoFe_2O_4$@PG ^{2nd} showed a decrease of 87.7% in relation to the initial concentration of aromatic compounds. Although the reaction conducted with $CoFe_2O_4$@PG ^{2nd} did not lead to the complete degradation of the aromatic compounds, the value obtained is still higher than the concentration decrease obtained for the reaction conducted with $CoFe_2O_4$@RF, which shows a decrease of 76% after 24 h, in relation to the initial concentration of aromatic compounds, Figure 23, thus evidencing that the $CoFe_2O_4$@PG catalyst presents a higher catalytic activity and stability even after three oxidation runs.

CONCLUSIONS AND FUTURE RESEARCH

5 CONCLUSIONS AND FUTURE RESEARCH

5.1 Conclusions

In this study, carbon-coated magnetic nanoparticles of cobalt ferrite ($CoFe_2O_4$) have been prepared by successive sol-gel for the bare core and through polymerization of phloroglucinol/glyoxylic acid (PG) and resorcinol/formaldehyde (RF) for the carbon-coating. Thereafter, the obtained materials were used as catalysts in the treatment of simulated wastewater containing paracetamol by CWPO. All catalysts studied in this work allow to reach 100% of paracetamol removal within 24 h of reaction time. However, different profiles of H_2O_2 decomposition and PCM removal were observed throughout the reaction. Complete removal of PCM was achieved within 6 h of reaction using the carbon-based nanoparticles as a catalyst while for the same interval of reaction time the uncoated catalyst showed only 47 % of paracetamol removal. In addition, pure adsorption runs showed a low contribution to the pollutant removal with a maximum decrease of initial concentration of PCM of 23.1%, suggesting that paracetamol is removed mainly by oxidative reaction.

In all the results considered, $CoFe_2O_4$@PG showed the best performance, due to the more controlled H_2O_2 decomposition profile and the gradual removal of paracetamol from the reaction system. The reutilization of $CoFe_2O_4$@PG in CWPO showed a similar trend in the second and third repetitions, reinforcing the potential application of the catalyst for real scenarios. The results obtained here for this system are encouraging to test the material considering different organic pollutants.

5.2 Future research

As suggestion for future research, it would be interesting to perform a deep study related to the chemistry surface and stability of $CoFe_2O_4$@RF and $CoFe_2O_4$@PG to elucidate the increased catalytic activity of the carbon-coated catalyst compared to the bare core. It is also necessary to perform TOC analysis and intermediates identification (e.g. by GC-MS), in order to verify the mineralization of PCM throughout the reaction and to establish reaction mechanisms. Transmission electron microscopy (TEM) analysis is also required to assess the morphology and structure of the developed material in order to confirm the formation of the carbon coating. Thereafter, the results obtained here for this system are encouraging to test the material considering different organic pollutants.

REFERENCES

6 REFERENCES

[1] J.J.R. Márquez, I. Levchuk, M. Sillanpää, Application of catalytic wet peroxide oxidation for industrial and urban wastewater treatment: A review, Catalysts. 8 (2018) 673–691. https://doi.org/10.3390/catal8120673.

[2] U.N.W.W.A.P. WWAP, The United Nations World Water Development Report 2017. Wastewater: The Untapped Resource. Paris, UNESCO, 2017.

[3] H.B. Quesada, A.T.A. Baptista, L.F. Cusioli, D. Seibert, C. de Oliveira Bezerra, R. Bergamasco, Surface water pollution by pharmaceuticals and an alternative of removal by low-cost adsorbents: A review, Chemosphere. 222 (2019) 766–780. https://doi.org/10.1016/j.chemosphere.2019.02.009.

[4] I. Sirés, E. Brillas, Remediation of water pollution caused by pharmaceutical residues based on electrochemical separation and degradation technologies: A review, Environ. Int. 40 (2012) 212–229. https://doi.org/10.1016/j.envint.2011.07.012.

[5] B. Jain, A.K. Singh, H. Kim, E. Lichtfouse, V.K. Sharma, Treatment of organic pollutants by homogeneous and heterogeneous Fenton reaction processes, Environ. Chem. Lett. 16 (2018) 947–967. https://doi.org/10.1007/s10311-018-0738-3.

[6] Y. Huaccallo-Aguilar, J.L. Diaz de Tuesta, S. Álvarez-Torrellas, H.T. Gomes, M. Larriba, G. Ovejero, J. García, New insights on the removal of diclofenac and ibuprofen by CWPO using a magnetite-based catalyst in an up-flow fixed-bed reactor, J. Environ. Manage. 281 (2021). https://doi.org/10.1016/j.jenvman.2020.111913.

[7] B. Tiwari, B. Sellamuthu, Y. Ouarda, P. Drogui, R.D. Tyagi, G. Buelna, Review on fate and mechanism of removal of pharmaceutical pollutants from wastewater using biological approach, Bioresour. Technol. 224 (2017) 1–12. https://doi.org/10.1016/j.biortech.2016.11.042.

[8] X. Qu, P.J.J. Alvarez, Q. Li, Applications of nanotechnology in water and wastewater treatment, Water Res. 47 (2013) 3931–3946.

https://doi.org/10.1016/j.watres.2012.09.058.

[9] T. Almeida, Nanopartículas Magnéticas e sua aplicaçãço no tratamento do câncer de mama, Univ. Fed. Ouro Preto. (2018) 1–9.

[10] T. Vangijzegem, D. Stanicki, S. Laurent, Magnetic iron oxide nanoparticles for drug delivery: applications and characteristics, Expert Opin. Drug Deliv. 16 (2019) 69–78. https://doi.org/10.1080/17425247.2019.1554647.

[11] V.F. Cardoso, A. Francesko, C. Ribeiro, M. Bañobre-López, P. Martins, S. Lanceros-Mendez, Advances in Magnetic Nanoparticles for Biomedical Applications, Adv. Healthc. Mater. 7 (2018) 1–35. https://doi.org/10.1002/adhm.201700845.

[12] B. Bethi, S.H. Sonawane, B.A. Bhanvase, S.P. Gumfekar, Nanomaterials-based advanced oxidation processes for wastewater treatment: A review, Chem. Eng. Process. Process Intensif. 109 (2016) 178–189. https://doi.org/10.1016/j.cep.2016.08.016.

[13] L. Mohammed, H.G. Gomaa, D. Ragab, J. Zhu, Magnetic nanoparticles for environmental and biomedical applications: A review, Particuology. 30 (2017) 1–14. https://doi.org/10.1016/j.partic.2016.06.001.

[14] S.C.N. Tang, I.M.C. Lo, Magnetic nanoparticles: Essential factors for sustainable environmental applications, Water Res. 47 (2013) 2613–2632. https://doi.org/10.1016/j.watres.2013.02.039.

[15] A.H. Lu, E.L. Salabas, F. Schüth, Magnetic nanoparticles: Synthesis, protection, functionalization, and application, Angew. Chemie - Int. Ed. 46 (2007) 1222–1244. https://doi.org/10.1002/anie.200602866.

[16] B. Issa, I.M. Obaidat, B.A. Albiss, Y. Haik, Magnetic nanoparticles: Surface effects and properties related to biomedicine applications, Int. J. Mol. Sci. 14 (2013) 21266–21305. https://doi.org/10.3390/ijms141121266.

[17] A.S. Silva, L. Diaz, S. Berberich, F.L. Deepak, M. Bañobre-lópez, Doxorubicin delivery performance of superparamagnetic carbon multi-core shell nanoparticles: pH dependence, stability and kinetic insight, Nanoscale. (2022) 7220–7232. https://doi.org/10.1039/d1nr08550f.

[18] M. Priebe, K.M. Fromm, Nanorattles or yolk-shell nanoparticles-what are they,

how are they made, and what are they good for?, Chem. - A Eur. J. 21 (2014) 3854–3874. https://doi.org/10.1002/chem.201405285.

[19] B. Mues, E.M. Buhl, T. Schmitz-Rode, I. Slabu, Towards optimized MRI contrast agents for implant engineering: Clustering and immobilization effects of magnetic nanoparticles, J. Magn. Magn. Mater. 471 (2019) 432–438. https://doi.org/10.1016/j.jmmm.2018.09.119.

[20] A. Avasthi, C. Caro, E. Pozo-Torres, M.P. Leal, M.L. García-Martín, Magnetic Nanoparticles as MRI Contrast Agents, Springer International Publishing, 2020. https://doi.org/10.1007/s41061-020-00302-w.

[21] M. Munoz, Z.M. de Pedro, J.A. Casas, J.J. Rodriguez, Preparation of magnetite-based catalysts and their application in heterogeneous Fenton oxidation - A review, Appl. Catal. B Environ. 176–177 (2015) 249–265. https://doi.org/10.1016/j.apcatb.2015.04.003.

[22] Z.B. Shifrina, V.G. Matveeva, L.M. Bronstein, Role of Polymer Structures in Catalysis by Transition Metal and Metal Oxide Nanoparticle Composites, Chem. Rev. 120 (2020) 1350–1396. https://doi.org/10.1021/acs.chemrev.9b00137.

[23] A.M. El-Toni, M.A. Habila, J.P. Labis, Z.A. Alothman, M. Alhoshan, A.A. Elzatahry, F. Zhang, Design, synthesis and applications of core-shell, hollow core, and nanorattle multifunctional nanostructures, Nanoscale. 8 (2016) 2510–2531. https://doi.org/10.1039/c5nr07004j.

[24] A. Wróblewska, E. Makuch, J. Młodzik, B. Michalkiewicz, Fe-carbon nanoreactors obtained from molasses as efficient catalysts for limonene oxidation, Green Process. Synth. 6 (2017) 397–401. https://doi.org/10.1515/gps-2016-0148.

[25] R.S. Ribeiro, R.O. Rodrigues, A.M.T. Silva, P.B. Tavares, A.M.C. Carvalho, J.L. Figueiredo, J.L. Faria, H.T. Gomes, Hybrid magnetic graphitic nanocomposites towards catalytic wet peroxide oxidation of the liquid effluent from a mechanical biological treatment plant for municipal solid waste, Appl. Catal. B Environ. 219 (2017) 645–657. https://doi.org/10.1016/j.apcatb.2017.08.013.

[26] M. Wang, Y. Boyjoo, J. Pan, S. Wang, J. Liu, Advanced yolk-shell nanoparticles as nanoreactors for energy conversion, Cuihua Xuebao/Chinese J. Catal. 38 (2017) 970–990. https://doi.org/10.1016/S1872-2067(17)62818-3.

[27] S. Behrens, I. Appel, Magnetic nanocomposites, Curr. Opin. Biotechnol. 39 (2016) 89–96. https://doi.org/10.1016/j.copbio.2016.02.005.

[28] M.B. Gawande, A. Goswami, T. Asefa, H. Guo, A. V. Biradar, D.L. Peng, R. Zboril, R.S. Varma, Core-shell nanoparticles: synthesis and applications in catalysis and electrocatalysis, Chem. Soc. Rev. 44 (2015) 7540–7590. https://doi.org/10.1039/c5cs00343a.

[29] J. Hu, M. Chen, X. Fang, L. Wu, Fabrication and application of inorganic hollow spheres, Chem. Soc. Rev. 40 (2011) 5472–5491. https://doi.org/10.1039/c1cs15103g.

[30] J. Liu, S.Z. Qiao, Q.H. Hu, G.Q. Lu, Magnetic nanocomposites with mesoporous structures: Synthesis and applications, Small. 7 (2011) 425–443. https://doi.org/10.1002/smll.201001402.

[31] J. Kim, H.S. Kim, N. Lee, T. Kim, H. Kim, T. Yu, I.C. Song, W.K. Moon, T. Hyeon, Multifunctional uniform nanoparticles composed of a magnetite nanocrystal core and a mesoporous silica shell for magnetic resonance and fluorescence imaging and for drug delivery, Angew. Chemie - Int. Ed. 47 (2008) 8438–8441. https://doi.org/10.1002/anie.200802469.

[32] J. Liu, H.Q. Yang, F. Kleitz, Z.G. Chen, T. Yang, E. Strounina, G.Q. Lu, S.Z. Qiao, Yolk-shell hybrid materials with a periodic mesoporous organosilica shell: Ideal nanoreactors for selective alcohol oxidation, Adv. Funct. Mater. 22 (2012) 591–599. https://doi.org/10.1002/adfm.201101900.

[33] C. Matei Ghimbeu, L. Vidal, L. Delmotte, J.M. Le Meins, C. Vix-Guterl, Catalyst-free soft-template synthesis of ordered mesoporous carbon tailored using phloroglucinol/glyoxylic acid environmentally friendly precursors, Green Chem. 16 (2014) 3079–3088. https://doi.org/10.1039/c4gc00269e.

[34] H. Yu, H. Zhang, H. Huang, Y. Liu, H. Li, H. Ming, Z. Kang, ZnO/carbon quantum dots nanocomposites: One-step fabrication and superior photocatalytic ability for toxic gas degradation under visible light at room temperature, New J. Chem. 36 (2012) 1031–1035. https://doi.org/10.1039/c2nj20959d.

[35] M. Sopronyi, F. Sima, C. Vaulot, L. Delmotte, A. Bahouka, C.M. Ghimbeu, Direct synthesis of graphitic mesoporous carbon from green phenolic resins exposed to

subsequent UV and IR laser irradiations, Sci. Rep. 6 (2016) 1–13. https://doi.org/10.1038/srep39617.

[36] R.T. Mayes, C. Tsouris, J.O. Kiggans, S.M. Mahurin, D.W. Depaoli, S. Dai, Hierarchical ordered mesoporous carbon from phloroglucinol-glyoxal and its application in capacitive deionization of brackish water, J. Mater. Chem. 20 (2010) 8674–8678. https://doi.org/10.1039/c0jm01911a.

[37] W. xin Jiang, W. Zhang, B. jing Li, J. Duan, Y. Lv, W. dong Liu, W. chi Ying, Combined fenton oxidation and biological activated carbon process for recycling of coking plant effluent, J. Hazard. Mater. 189 (2011) 308–314. https://doi.org/10.1016/j.jhazmat.2011.02.037.

[38] A.R. Ribeiro, O.C. Nunes, M.F.R. Pereira, A.M.T. Silva, An overview on the advanced oxidation processes applied for the treatment of water pollutants defined in the recently launched Directive 2013/39/EU, Environ. Int. 75 (2015) 33–51. https://doi.org/10.1016/j.envint.2014.10.027.

[39] R.S. Ribeiro, A.M.T. Silva, J.L. Figueiredo, J.L. Faria, H.T. Gomes, Catalytic wet peroxide oxidation: A route towards the application of hybrid magnetic carbon nanocomposites for the degradation of organic pollutants. A review, Appl. Catal. B Environ. 187 (2016) 428–460. https://doi.org/10.1016/j.apcatb.2016.01.033.

[40] R. Dewil, D. Mantzavinos, I. Poulios, M.A. Rodrigo, New perspectives for Advanced Oxidation Processes, J. Environ. Manage. 195 (2017) 93–99. https://doi.org/10.1016/j.jenvman.2017.04.010.

[41] E. Neyens, J. Baeyens, A review of classic Fenton's peroxidation as an advanced oxidation technique, J. Hazard. Mater. 98 (2003) 33–50. https://doi.org/10.1016/S0304-3894(02)00282-0.

[42] S. Chaliha, K.G. Bhattacharyya, Using Mn(II)- MCM41 as an environment-friendly catalyst to oxidize phenol, 2-chlorophenol, and 2-nitrophenol in aqueous solution, Ind. Eng. Chem. Res. 47 (2008) 1370–1379. https://doi.org/10.1021/ie071075f.

[43] A. Matilainen, M. Sillanpää, Removal of natural organic matter from drinking water by advanced oxidation processes, Chemosphere. 80 (2010) 351–365. https://doi.org/10.1016/j.chemosphere.2010.04.067.

[44] J. Mu, S. Li, J. Wang, X. Li, W. Chen, X. Tong, Y. Tang, L. Li, Efficient catalytic ozonation of bisphenol A by three-dimensional mesoporous CeOx-loaded SBA-16, Chemosphere. 278 (2021). https://doi.org/10.1016/j.chemosphere.2021.130412.

[45] M.M. M'Arimi, C.A. Mecha, A.K. Kiprop, R. Ramkat, Recent trends in applications of advanced oxidation processes (AOPs) in bioenergy production: Review, Renew. Sustain. Energy Rev. 121 (2020) 109669. https://doi.org/10.1016/j.rser.2019.109669.

[46] M. Munoz, J. Nieto-Sandoval, E. Serrano, Z.M. De Pedro, J.A. Casas, CWPO intensification by induction heating using magnetite as catalyst, J. Environ. Chem. Eng. 8 (2020) 104085. https://doi.org/10.1016/j.jece.2020.104085.

[47] N. Inchaurrondo, J. Cechini, J. Font, P. Haure, Strategies for enhanced CWPO of phenol solutions, Appl. Catal. B Environ. 111–112 (2012) 641–648. https://doi.org/10.1016/j.apcatb.2011.11.019.

[48] N. Wang, T. Zheng, G. Zhang, P. Wang, A review on Fenton-like processes for organic wastewater treatment, J. Environ. Chem. Eng. 4 (2016) 762–787. https://doi.org/10.1016/j.jece.2015.12.016.

[49] H. Qin, R. Xiao, W. Shi, Y. Wang, H. Li, L. Guo, H. Cheng, J. Chen, Magnetic core-shell-structured Fe3O4@CeO2 as an efficient catalyst for catalytic wet peroxide oxidation of benzoic acid, RSC Adv. 8 (2018) 33972–33979. https://doi.org/10.1039/c8ra07144f.

[50] H. Zhao, H.J. Cui, M.L. Fu, Synthesis of core-shell structured Fe3O4 at α-MnO2 microspheres for efficient catalytic degradation of ciprofloxacin, RSC Adv. 4 (2014) 39472–39475. https://doi.org/10.1039/c4ra06696k.

[51] J.A. Melero, F. Martínez, J.A. Botas, R. Molina, M.I. Pariente, Heterogeneous catalytic wet peroxide oxidation systems for the treatment of an industrial pharmaceutical wastewater, Water Res. 43 (2009) 4010–4018. https://doi.org/10.1016/j.watres.2009.04.012.

[52] A. Rey, M. Faraldos, J.A. Casas, J.A. Zazo, A. Bahamonde, J.J. Rodríguez, Catalytic wet peroxide oxidation of phenol over Fe/AC catalysts: Influence of iron precursor and activated carbon surface, Appl. Catal. B Environ. 86 (2009) 69–77.

https://doi.org/10.1016/j.apcatb.2008.07.023.

[53] A.S. Silva, M.S. Kalmakhanova, B.K. Massalimova, J.L.D. de Tuesta, H.T. Gomes, Wet peroxide oxidation of paracetamol using acid activated and Fe/Co-pillared clay catalysts prepared from natural clays, Catalysts. 9 (2019). https://doi.org/10.3390/catal9090705.

[54] Q.C. Do, D.G. Kim, S.O. Ko, Insights into heterogeneous Fenton-like systems catalyzed by novel magnetic yolk-shell structures for the removal of acetaminophen from aquatic environments, J. Water Process Eng. 32 (2019) 100980. https://doi.org/10.1016/j.jwpe.2019.100980.

[55] J.H. Ramirez, F.J. Maldonado-Hódar, A.F. Pérez-Cadenas, C. Moreno-Castilla, C.A. Costa, L.M. Madeira, Azo-dye Orange II degradation by heterogeneous Fenton-like reaction using carbon-Fe catalysts, Appl. Catal. B Environ. 75 (2007) 312–323. https://doi.org/10.1016/j.apcatb.2007.05.003.

[56] E.G. Garrido-Ramírez, B.K.G. Theng, M.L. Mora, Clays and oxide minerals as catalysts and nanocatalysts in Fenton-like reactions - A review, Appl. Clay Sci. 47 (2010) 182–192. https://doi.org/10.1016/j.clay.2009.11.044.

[57] A. Venault, Y. Liu, J. Wu, H. Yang, Y. Chang, OATAO is an open access repository that collects the work of Toulouse researchers and makes it freely available over the web where possible This is an author ' s version published in : http://oatao.univ-toulouse.fr/20270 Official URL : https://dx.doi.org/, 1 (2014).

[58] R.S. Ribeiro, J. Gallo, M. Bañobre-López, A.M.T. Silva, J.L. Faria, H.T. Gomes, Enhanced performance of cobalt ferrite encapsulated in graphitic shell by means of AC magnetically activated catalytic wet peroxide oxidation of 4-nitrophenol, Chem. Eng. J. 376 (2019) 120012. https://doi.org/10.1016/j.cej.2018.09.173.

[59] M. Khodadadi, A. Hossein Panahi, T.J. Al-Musawi, M.H. Ehrampoush, A.H. Mahvi, The catalytic activity of FeNi3@SiO2 magnetic nanoparticles for the degradation of tetracycline in the heterogeneous Fenton-like treatment method, J. Water Process Eng. 32 (2019) 100943. https://doi.org/10.1016/j.jwpe.2019.100943.

[60] Y. Huaccallo-Aguilar, S. Álvarez-Torrellas, M. Larriba, V.I. Águeda, J.A. Delgado, G. Ovejero, J. García, Optimization parameters, kinetics and mechanism

of naproxen removal by catalytic wet peroxide oxidation with a hybrid iron-based magnetic catalyst, Catalysts. 9 (2019) 1–23. https://doi.org/10.3390/catal9030287.

[61] N. Barrios-Bermúdez, M. González-Avendaño, I. Lado-Touriño, A. Cerpa-Naranjo, M.L. Rojas-Cervantes, Fe-Cu doped multiwalled carbon nanotubes for fenton-like degradation of paracetamol under mild conditions, Nanomaterials. 10 (2020) 11–13. https://doi.org/10.3390/nano10040749.

[62] H. Niu, Dizhang, Z. Meng, Y. Cai, Fast defluorination and removal of norfloxacin by alginate/Fe@Fe 3O 4 core/shell structured nanoparticles, J. Hazard. Mater. 227–228 (2012) 195–203. https://doi.org/10.1016/j.jhazmat.2012.05.036.

[63] S.P. Sun, X. Zeng, A.T. Lemley, Nano-magnetite catalyzed heterogeneous Fenton-like degradation of emerging contaminants carbamazepine and ibuprofen in aqueous suspensions and montmorillonite clay slurries at neutral pH, J. Mol. Catal. A Chem. 371 (2013) 94–103. https://doi.org/10.1016/j.molcata.2013.01.027.

[64] S.E. Shirsath, D. Wang, S.S. Jadhav, M.L. Mane, S. Li, Ferrites obtained by sol-gel method, 2018. https://doi.org/10.1007/978-3-319-32101-1_125.

[65] T. Giannakopoulou, L. Kompotiatis, A. Kontogeorgakos, G. Kordas, Microwave behavior of ferrites prepared via sol-gel method, J. Magn. Magn. Mater. 246 (2002) 360–365. https://doi.org/10.1016/S0304-8853(02)00106-3.

[66] M. Karimi, J.L. Diaz de Tuesta, C.N. Carmem, H.T. Gomes, A.E. Rodrigues, J.A.C. Silva, Compost from Municipal Solid Wastes as a Source of Biochar for CO2 Capture, Chem. Eng. Technol. 43 (2020) 1336–1349. https://doi.org/10.1002/ceat.201900108.

[67] M. Thommes, K. Kaneko, A. V. Neimark, J.P. Olivier, F. Rodriguez-Reinoso, J. Rouquerol, K.S.W. Sing, Physisorption of gases, with special reference to the evaluation of surface area and pore size distribution (IUPAC Technical Report), Pure Appl. Chem. 87 (2015) 1051–1069. https://doi.org/10.1515/pac-2014-1117.

[68] L.F. Sanches, Valorisation of carbon-rich solid wastes into nanostructured catalysts for wet peroxide oxidation of contaminants of emerging concern, (2021).

[69] G.M. Eisenberg, Colorimetric Determination of Hydrogen Peroxide, Ind. Eng. Chem. - Anal. Ed. 15 (1943) 327–328. https://doi.org/10.1021/i560117a011.

[70] J. H.Alonson, T.. Antón, T.. Montero, Análisis químico de aguas residuales, 2004.

[71] Z. Mohammadi, N. Attaran, A. Sazgarnia, S.A.M. Shaegh, A. Montazerabadi, Superparamagnetic cobalt ferrite nanoparticles as T2 contrast agent in MRI: In vitro study, IET Nanobiotechnology. 14 (2020) 396–404. https://doi.org/10.1049/iet-nbt.2019.0210.

[72] W.J. Liu, Y.X. Liu, X.Y. Yan, G.P. Yong, Y.P. Xu, S.M. Liu, One-pot synthesis of yolk-shell mesoporous carbon spheres with high magnetisation, J. Mater. Chem. A. 2 (2014) 9600–9606. https://doi.org/10.1039/c4ta01088d.

[73] I. Prakash, N. Nallamuthu, P. Muralidharan, M. Venkateswarlu, N. Satyanarayana, Synthesis of SiO2/CoFe2O4 nanocomposite by base catalyst assisted in-situ sol-gel process, AIP Conf. Proc. 1276 (2010) 227–232. https://doi.org/10.1063/1.3504302.

[74] J. Lee, S. Han, T. Hyeon, Synthesis of new nanoporous carbon materials using nanostructured silica materials as templates, J. Mater. Chem. (2004) 478–486. https://doi.org/10.1039/b311541k.

[75] J. Xu, A. Wang, T. Zhang, A two-step synthesis of ordered mesoporous resorcinol-formaldehyde polymer and carbon, Carbon N. Y. 50 (2012) 1807–1816. https://doi.org/10.1016/j.carbon.2011.12.028.

[76] N. Villota, J.M. Lomas, L.M. Camarero, Study of the paracetamol degradation pathway that generates color and turbidity in oxidized wastewaters by photo-Fenton technology, J. Photochem. Photobiol. A Chem. 329 (2016) 113–119. https://doi.org/10.1016/j.jphotochem.2016.06.024.

[77] Y. Cheng, H. Sun, W. Jin, N. Xu, Photocatalytic degradation of 4-chlorophenol with combustion synthesized TiO2 under visible light irradiation, Chem. Eng. J. 128 (2007) 127–133. https://doi.org/10.1016/j.cej.2006.09.009.

[78] D. Vogna, R. Marotta, A. Napolitano, M. D'Ischia, Advanced oxidation chemistry of paracetamol. UV/H2O2-induced hydroxylation/degradation pathways and 15N-aided inventory of nitrogenous breakdown products, J. Org. Chem. 67 (2002) 6143–6151. https://doi.org/10.1021/jo025604v.

[79] L.C. Almeida, S. Garcia-Segura, N. Bocchi, E. Brillas, Solar photoelectro-Fenton degradation of paracetamol using a flow plant with a Pt/air-diffusion cell coupled with a compound parabolic collector: Process optimization by response surface

methodology, Appl. Catal. B Environ. 103 (2011) 21–30. https://doi.org/10.1016/j.apcatb.2011.01.003.

[80] F. Velichkova, C. Julcour-Lebigue, B. Koumanova, H. Delmas, Heterogeneous Fenton oxidation of paracetamol using iron oxide (nano)particles, J. Environ. Chem. Eng. 1 (2013) 1214–1222. https://doi.org/10.1016/j.jece.2013.09.011.

[81] R.S. Ribeiro, A.M.T. Silva, J.L. Figueiredo, J.L. Faria, H.T. Gomes, The influence of structure and surface chemistry of carbon materials on the decomposition of hydrogen peroxide, Carbon N. Y. 62 (2013) 97–108. https://doi.org/10.1016/j.carbon.2013.06.001.

[82] A. SOUFI, H. HAJJAOUI, R. ELMOUBARKI, M. ABDENNOURI, S. QOURZAL, N. BARKA, Spinel ferrites nanoparticles: Synthesis methods and application in heterogeneous Fenton oxidation of organic pollutants – A review, Appl. Surf. Sci. Adv. 6 (2021) 100145. https://doi.org/10.1016/j.apsadv.2021.100145.